Joint Transmit and Receive Filter Optimization for Sub-Nyquist Wireless Channel Estimation

Andreas Lenz, Manuel S. Stein, A. Lee Swindlehurst

arXiv:1704.07612v1 [cs.IT] 25 Apr 2017

***Abstract*—In this article a framework is presented for the joint optimization of the analog transmit and receive filter with respect to a channel estimation problem. At the receiver, conventional signal processing systems restrict the bandwidth of the analog pre-filter B to the rate of the analog-to-digital converter f_s in order to comply with the well-known Nyquist sampling theorem. In contrast, here we consider a transceiver that by design violates the common paradigm $B \leq f_s$. To this end, at the receiver we allow for a higher pre-filter bandwidth $B > f_s$ and study the achievable channel estimation accuracy under a fixed sampling rate when the transmit and receive filter are jointly optimized with respect to the Bayesian Cramér-Rao lower bound. For the case of a channel with unknown delay-Doppler shift we show how to approximate the required Fisher information matrix and solve the transceiver design problem by an alternating optimization algorithm. The presented approach allows us to explore the Pareto-optimal region spanned by transmit and receive filters which are favorable under a weighted mean squared error criterion. We discuss the complexity of the obtained transceiver design by visualizing the resulting ambiguity function. Finally, we verify the achievable performance of the proposed designs by Monte-Carlo simulations of a likelihood-based channel estimator.**

***Index Terms*—ambiguity function, Bayesian Cramér-Rao lower bound, channel estimation, compressive sensing, delay-Doppler shift, Fisher information, sub-Nyquist sampling, transceiver optimization, waveform design, wireless systems**

I. Introduction

THE inference of unknown channel parameters is of interest in technical applications such as radar, sonar, communication, image analysis, biomedicine or seismology. In radar systems knowledge of the delay-Doppler shift can be used to precisely determine the distance and velocity of a target object, while in wireless communication, channel estimation is required in order to adapt the transmission rate to the channel capacity. For imaging and biomedical applications conclusions about the test medium can be drawn from precise measurements of the received signal parameters.

During the design of such systems, resource and hardware restrictions, e.g. power consumption and computational effort, have to be taken into consideration and a favorable trade-off between high system performance and low system complexity has to be found. With respect to the analog hardware costs at the receiver side, the sampling rate of the analog-to-digital (A/D) conversion process has been identified as a bottleneck [1], [2]. When the receive system is designed under the prevailing requirement of fulfilling the Nyquist sampling theorem, i.e., the analog pre-filter bandlimits the sensor signal to the A/D conversion rate, the achievable sampling rate f_s at the receiver restricts the two-sided bandwidth B of the transmitter and therefore the overall system performance. While by choosing $B \leq f_s$ the sampling theorem guarantees perfect reconstruction of the band-limited analog receive signal from its digital samples, for channel estimation we are instead interested in the recovery of just a few signal parameters using a probabilistic model-based approach. Since channel estimation accuracy rather than signal reconstruction is the desired goal, compliance with the sampling theorem can be relaxed. This leads to the question of how to design channel estimation methods when commonly used principles like the sampling theorem are set aside.

A. Lenz is with the Institute for Communications Engineering, Technical University of Munich (TUM), Germany (e-mail: andreas.lenz@mytum.de). M. S. Stein is with the Mathematics Department (DWIS), Vrije Universiteit Brussel (VUB), Belgium (e-mail: manuel.stein@vub.ac.be). A. L. Swindlehurst is with the Center for Pervasive Communications and Computing (CPCC), University of California (UCI), Irvine, CA 92697 USA (e-mail: swindle@uci.edu).

II. Problem Formulation

A. Generic System Model

Consider the baseband system model in Fig. 1. A periodic

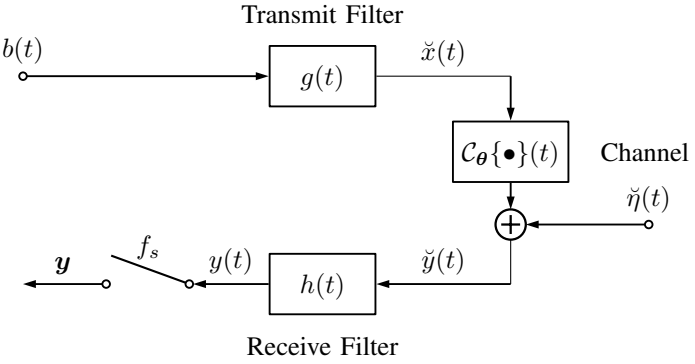

Fig. 1. System Model (Baseband Representation)

analog transmit waveform $\breve{x}(t) \in \mathbb{C}$ is generated by feeding the filter $g(t) \in \mathbb{C}$ of bandwidth B with a train of impulses

$$b(t) = \sum_{m=-\infty}^{\infty} \delta(t - mT_0), \tag{1}$$

where $\delta(t)$ denotes the Dirac function, such that

$$\breve{x}(t) = b(t) * g(t), \tag{2}$$

with the convolution operator '$*$'. The transmit signal (2) propagates through the channel $\mathcal{C}_{\boldsymbol{\theta}}\{\bullet\}(t)$, depicted by a functional operator with parameters $\boldsymbol{\theta} \in \mathbb{R}^D$. The channel output is

assumed to be perturbed by additive white Gaussian noise $\breve{\eta}(t) \in \mathbb{C}$ with constant power spectral density N_0, such that

$$\breve{y}(t) = \mathcal{C}_{\boldsymbol{\theta}}\{\breve{x}\}(t) + \breve{\eta}(t). \tag{3}$$

The signal $\breve{y}(t) \in \mathbb{C}$ is filtered by a linear, time-invariant filter $h(t) \in \mathbb{C}$, such that the final analog receive signal

$$\begin{aligned} y(t) &= \big(\mathcal{C}_{\boldsymbol{\theta}}\{\breve{x}\}(t) + \breve{\eta}(t)\big) * h(t) \\ &= v(t;\boldsymbol{\theta}) + \eta(t) \end{aligned} \tag{4}$$

is obtained.

The signal $y(t) \in \mathbb{C}$ is sampled in intervals of $T_s = \frac{1}{f_s}$ for the duration T_0, resulting in $N = \frac{T_0}{T_s} \in \mathbb{Z}_+$ samples

$$\boldsymbol{y} = \boldsymbol{v}(\boldsymbol{\theta}) + \boldsymbol{\eta}, \tag{5}$$

where we use vector notation in order to summarize N samples

$$\boldsymbol{u} = \left[u\left(-\frac{N}{2}T_s\right), \ldots, u\left(\left(\frac{N}{2}-1\right)T_s\right)\right]^{\mathrm{T}} \in \mathbb{C}^N \tag{6}$$

of an analog waveform $u(t) \in \mathbb{C}$ and $t \in [-\frac{T_0}{2}, \frac{T_0}{2})$. We assume that the noise samples $\boldsymbol{\eta} \in \mathbb{C}^N$ in (5) follow a zero-mean Gaussian distribution with covariance matrix

$$\boldsymbol{R}_{\boldsymbol{\eta}} = \mathrm{E}_{\boldsymbol{\eta}}[\boldsymbol{\eta}\boldsymbol{\eta}^{\mathrm{H}}] \in \mathbb{C}^{N\times N}. \tag{7}$$

B. Channel Parameter Estimation

Throughout this work a pilot-based Bayesian estimation approach is assumed, i.e., the receiver has perfect knowledge about the transmit filter $g(t)$, the form of the channel operator $\mathcal{C}_{\boldsymbol{\theta}}\{\bullet\}(t)$, the receive filter $h(t)$ and the sampling rate f_s. Therefore, the exact channel model $p(\boldsymbol{y}|\boldsymbol{\theta})$ is available at the receiver, while the channel parameters $\boldsymbol{\theta}$ are assumed to be unknown random variables distributed according to a known prior probability law $\boldsymbol{\theta} \sim p(\boldsymbol{\theta})$.

The goal of the receiver is to infer the unknown channel parameters $\boldsymbol{\theta}$ based on the received digital data $\boldsymbol{y}$ using an appropriate channel estimation algorithm $\hat{\boldsymbol{\theta}}(\boldsymbol{y})$. The weighted estimation error of $\hat{\boldsymbol{\theta}}(\boldsymbol{y})$ is defined as

$$\mathrm{MSE}(\boldsymbol{M}) = \mathrm{tr}\big(\boldsymbol{M}\boldsymbol{R}_{\boldsymbol{\epsilon}}\big), \tag{8}$$

for some positive semidefinite weighting matrix $\boldsymbol{M} \in \mathbb{R}^{D\times D}$ where we define the mean squared error (MSE) matrix

$$\boldsymbol{R}_{\boldsymbol{\epsilon}} = \mathrm{E}_{\boldsymbol{y},\boldsymbol{\theta}}\Big[\big(\hat{\boldsymbol{\theta}}(\boldsymbol{y}) - \boldsymbol{\theta}\big)\big(\hat{\boldsymbol{\theta}}(\boldsymbol{y}) - \boldsymbol{\theta}\big)^{\mathrm{T}}\Big]. \tag{9}$$

As a direct computation of the MSE matrix (9) is generally intractable, a performance analysis is usually based on the Bayesian Cramér-Rao lower bound (BCRLB) [3, p. 5]

$$\boldsymbol{R}_{\boldsymbol{\epsilon}} \geq \big(\boldsymbol{J}_D + \boldsymbol{J}_P\big)^{-1}, \tag{10}$$

which forms a fundamental limit for the achievable estimation accuracy (9). The first term on the right-hand side of (10) represents the expected Fisher information matrix (EFIM)

$$\boldsymbol{J}_D = \mathrm{E}_{\boldsymbol{\theta}}\big[\boldsymbol{J}_F(\boldsymbol{\theta})\big], \tag{11}$$

with the Fisher information matrix (FIM) exhibiting entries

$$[\boldsymbol{J}_F(\boldsymbol{\theta})]_{ij} = -\mathrm{E}_{\boldsymbol{y}|\boldsymbol{\theta}}\left[\frac{\partial^2 \ln p(\boldsymbol{y}|\boldsymbol{\theta})}{\partial[\boldsymbol{\theta}]_i \partial[\boldsymbol{\theta}]_j}\right]. \tag{12}$$

The matrix (11) characterizes the averaged amount of information about the parameters $\boldsymbol{\theta}$ that is embodied in the noisy receive data $\boldsymbol{y}$. For the Gaussian signal model (5), the FIM entries (12) are given by [4, p. 525]

$$[\boldsymbol{J}_F(\boldsymbol{\theta})]_{ij} = 2\mathrm{Re}\left\{\left(\frac{\partial \boldsymbol{v}(\boldsymbol{\theta})}{\partial[\boldsymbol{\theta}]_i}\right)^{\mathrm{H}} \boldsymbol{R}_{\boldsymbol{\eta}}^{-1}\left(\frac{\partial \boldsymbol{v}(\boldsymbol{\theta})}{\partial[\boldsymbol{\theta}]_j}\right)\right\}. \tag{13}$$

The second summand in (10) is the prior information matrix (PIM) with entries

$$[\boldsymbol{J}_P]_{ij} = -\mathrm{E}_{\boldsymbol{\theta}}\left[\frac{\partial^2 \ln p(\boldsymbol{\theta})}{\partial[\boldsymbol{\theta}]_i \partial[\boldsymbol{\theta}]_j}\right]. \tag{14}$$

It specifies the information about the unknown parameters which is contained in $p(\boldsymbol{\theta})$.

Accessing and optimizing the system performance (9) based on a theoretical measure like the BCRLB (10) has the advantage that the achievable accuracy level can be computed analytically and therefore extensive simulations of the algorithm $\hat{\boldsymbol{\theta}}(\boldsymbol{y})$ are not required.

C. Transceiver Design Problem

The design problem of finding transmit and receive filters $\{g^\star(t), h^\star(t)\}$ that minimize the MSE (8) of the estimation algorithm $\hat{\boldsymbol{\theta}}(\boldsymbol{y})$ under a particular weighting $\boldsymbol{M}$, subject to a transmit power constraint P_T, can be formulated as

$$\min_{g(t),h(t)} \mathrm{tr}(\boldsymbol{M}\boldsymbol{R}_{\boldsymbol{\epsilon}}), \quad \text{s.t.} \quad \frac{1}{T_0}\int_{T_0} |\breve{x}(t)|^2 \mathrm{d}t \leq P_T. \tag{15}$$

Note that beside the transmit power constraint we assume an ideal transmit amplifier without further restrictions.

Under the assumption that a *Bayesian efficient estimator* $\hat{\boldsymbol{\theta}}(\boldsymbol{y})$ is available it holds that [3, p. 5]

$$\boldsymbol{R}_{\boldsymbol{\epsilon}} = \big(\boldsymbol{J}_D + \boldsymbol{J}_P\big)^{-1}. \tag{16}$$

Due to the fact that $\boldsymbol{J}_P$ is independent of both filters and $\boldsymbol{J}_P, \boldsymbol{J}_D$ are positive definite, (15) then simplifies to

$$\min_{g(t),h(t)} \mathrm{tr}(\boldsymbol{M}\boldsymbol{J}_D^{-1}), \quad \text{s.t.} \quad \frac{1}{T_0}\int_{T_0} |\breve{x}(t)|^2 \mathrm{d}t \leq P_T. \tag{17}$$

As the minimization over the inverse of $\boldsymbol{J}_D$ in (17) is difficult, an alternative optimization problem

$$\max_{g(t),h(t)} \mathrm{tr}(\boldsymbol{M'}\boldsymbol{J}_D), \quad \text{s.t.} \quad \frac{1}{T_0}\int_{T_0} |\breve{x}(t)|^2 \mathrm{d}t \leq P_T \tag{18}$$

can be considered. It can been shown that (18) is equivalent to (17) in a boundary preserving sense [5], i.e., if $\boldsymbol{J}_D^*$ is a solution of (18) with $\boldsymbol{M'}$, there exists a matrix $\boldsymbol{M}$ (not necessarily equal to $\boldsymbol{M'}$) for which the original optimization problem (17) has the solution $\boldsymbol{J}_D^{*,-1}$.

III. Contribution and Outline

For the example of a single-input single-output (SISO) channel with delay-Doppler shift, we develop a framework to solve the transceiver optimization problem (18) under the sub-Nyquist condition $B > f_s$.

After providing an overview on related work (Section IV), in particular we

- Introduce the wireless receive model with delay-Doppler shift and derive its FIM under arbitrary transmit and receive filters (Section V).
- Show how to approximate the information matrix $\boldsymbol{J}_F(\boldsymbol{\theta})$ and $\boldsymbol{J}_D$ in the frequency domain (Section VI).
- Provide an algorithm to solve the transceiver design problem (18) by alternating between optimizing the transmit $g(t)$ and the receive filter $h(t)$ (Section VIII).
- Characterize the approximate Pareto-optimal region obtained by jointly optimizing the transmit and receive filter $g(t)$ and $h(t)$ with respect to a weighted MSE criterion (Section X).
- Discuss the ambiguity function resulting from the optimized transceiver design (Section X).
- Verify the performance obtained under an optimized design by Monte-Carlo simulation of an asymptotically efficient algorithm $\hat{\boldsymbol{\theta}}(\boldsymbol{y})$ (Section XI).

Our final conclusions are outlined in Section XII. Note that preliminary results have been discussed in [6]–[8], where we have focused on either optimizing the receive or the transmit filter of a sub-Nyquist wireless system and [9] which was centered around a compressive sensing framework.

IV. Related Work

The analysis and optimization of transceiver systems enjoys significant attention in the signal processing community [10]–[13]. While for example [14], [15] focus on signal optimization for classical radar systems, waveform design of orthogonal frequency division multiplexing (OFDM) signals for radar applications have been considered in [16], [17]. The favorable design of satellite-based positioning signals with high time-delay estimation accuracy is discussed in [18]. Optimization of transmit and receive filters in the spatial domain plays a crucial role in multiple-input multiple-output (MIMO) radar systems [19], [20] and for cognitive radars, where high accuracy is achieved by using a Bayesian tracking algorithm and adapting the transmit signal to the state-space knowledge [21]. In [22] this concept is extended to MIMO radar systems which offer improved parameter identifiability and higher resolution [23] in comparison to phased arrays. Further, MIMO radar features the effect of virtual receive antennas [24], leading to high accuracy at lower hardware costs.

When performing the transceiver system optimization various figures of merit have been considered. In particular mutual information and signal-to-noise ratio (SNR) are popular metrics [12], [14], [15], [25], while a low mean squared error (MSE) for the estimated channel parameters is an alternative choice and leads to the use of estimation theoretic error bounds [22], [26], [27]. Further, the ambiguity function (AF) of a given transmit signal is a classical tool to characterize the waveform quality for applications where joint estimation of time-delay and frequency shift is desired [19], [28]–[32]. Subspace-based techniques for delay-Doppler estimation problems are presented in [33], [34] and lead to significant complexity reduction of the maximum likelihood (ML) estimator.

An important aspect in the context of this article is the field of compressed sensing (CS) and finite rate of innovation (FRI) techniques, where sparse signal structures [35] and signals with finite degrees of freedom [36] are exploited in order to facilitate signal processing. CS-related work focuses on methods for reconstructing signals that embody sparsity from a small number of samples [37], while FRI techniques attempt to reconstruct the original signal without bandwidth limitations [38]. In [39]–[41] reconstruction of FRI signals in noise is considered. The work of [42] describes CS methods for parameter estimation applications where perfect signal reconstruction is not required. Taking into account sampling hardware complexity, Xampling has been introduced as a multi-band sampling technique that allows signal processing at sampling rates far below the Nyquist rate [43], [44]. With this approach, low-rate analog-to-digital conversion architectures for radar systems have been proposed which exhibit the same estimation performance as receivers that operate at the Nyquist rate when the SNR is sufficiently high [45], [46]. Note that in contrast to these works, we consider system optimization under a classical baseband receiver architecture which operates at a sampling rate f_s smaller than the Nyquist bandwidth B.

V. Wireless Channel with Delay-Doppler Shift

A. Specific Channel Model

We consider a single-tap channel with delay-Doppler shift, such that

$$\mathcal{C}_{\boldsymbol{\theta}}\{\breve{x}\}(t) = \gamma \breve{x}(t-\tau)\mathrm{e}^{\mathrm{j}2\pi\nu t}, \tag{19}$$

with channel gain $\gamma \in \mathbb{C}$, time-delay $\tau \in \mathbb{R}$ and Doppler shift $\nu \in \mathbb{R}$. For the design problem (18), we assume that the linear channel gain γ is constant, such that the unknown random channel parameter vector is

$$\boldsymbol{\theta} = \begin{bmatrix} \tau & \nu \end{bmatrix}^{\mathrm{T}}. \tag{20}$$

Here we assume that the channel gain γ is known at the receiver, which simplifies the formulation of the transceiver optimization problem. However, when testing the optimized filters for a practical scenario in the last section we will treat γ to be deterministic unknown. In the following it is assumed that the channel parameters are Gaussian distributed

$$\boldsymbol{\theta} \sim \mathcal{N}(\mathbf{0}, \boldsymbol{R}_{\boldsymbol{\theta}}) \tag{21}$$

and stochastically independent, such that

$$\boldsymbol{R}_{\boldsymbol{\theta}} = \begin{bmatrix} \sigma_\tau^2 & 0 \\ 0 & \sigma_\nu^2 \end{bmatrix}. \tag{22}$$

B. Frequency Domain Representation

Solving the optimization problem (18) requires an analytical characterization of the EFIM (11) under the channel model (19). A frequency-domain representation enables a compact and insightful notation for the receive signal model [7], [47] and thus of the FIM entries (13).

For the derivation, we assume a fixed sampling rate f_s at the receiver. The transmit filter $g(t)$ is band-limited with two-sided bandwidth B. In contrast to the common assumption

$B \leq f_s$, in our setup we allow $B > f_s$. Due to periodicity, the waveform $\breve{x}(t)$ can be represented by its Fourier series

$$\breve{x}(t) = \sum_{k=-\frac{K}{2}}^{\frac{K}{2}-1} G_k \mathrm{e}^{\mathrm{j}k\omega_0 t}, \tag{23}$$

where $\omega_0 = \frac{2\pi}{T_0} = 2\pi f_0$. Note that $K = \lceil \frac{2\pi B}{\omega_0} \rceil \in \mathbb{N}$ is the total number of harmonics. G_k denotes the k-th Fourier coefficient of the transmit filter

$$G_k = \frac{1}{T_0} \int_{-\infty}^{\infty} g(t) \mathrm{e}^{\mathrm{j}k\omega_0 t} \mathrm{d}t. \tag{24}$$

We write $\mathcal{K}$ for the set of Fourier coefficient indices

$$\mathcal{K} = \Big\{ -\frac{K}{2}, -\frac{K}{2}+1, \ldots, \frac{K}{2}-1 \Big\} \tag{25}$$

with cardinality $|\,\mathcal{K}\,| = K$. Inserting expression (23) into (19) and applying the filtering operation in (4), we obtain

$$\begin{aligned} v(t;\boldsymbol{\theta}) &= \gamma \sum_{k\in\mathcal{K}} G_k \Big(\mathrm{e}^{\mathrm{j}k\omega_0(t-\tau)} \mathrm{e}^{\mathrm{j}2\pi\nu t} \Big) * h(t) \\ &= \gamma \mathrm{e}^{\mathrm{j}2\pi\nu t} \sum_{k\in\mathcal{K}} \mathrm{e}^{\mathrm{j}k\omega_0 t} \mathrm{e}^{-\mathrm{j}k\omega_0\tau} G_k H(k\omega_0 + 2\pi\nu), \end{aligned} \tag{26}$$

where

$$H(\omega) = \int_{-\infty}^{\infty} h(t) \mathrm{e}^{-\mathrm{j}\omega t} \mathrm{d}t \tag{27}$$

is the Fourier transform of the receive filter $h(t)$. Evaluating $v(t;\boldsymbol{\theta})$ at sampling instants $nT_s, n \in \{-\frac{N}{2}, \ldots, \frac{N}{2}-1\}$ yields

$$\begin{aligned} v(nT_s;\boldsymbol{\theta}) =& \gamma \mathrm{e}^{\mathrm{j}2\pi\nu n T_s} \sum_{k\in\mathcal{K}} \mathrm{e}^{\mathrm{j}2\pi\frac{kn}{N}} \mathrm{e}^{-\mathrm{j}k\omega_0\tau} G_k H(k\omega_0 + 2\pi\nu) \\ =& \gamma \mathrm{e}^{\mathrm{j}2\pi\nu n T_s} \sum_{k=-\frac{N}{2}}^{\frac{N}{2}-1} \mathrm{e}^{\mathrm{j}2\pi\frac{kn}{N}} \sum_{l=-L_n(k)}^{L_p(k)} \mathrm{e}^{-\mathrm{j}(k\omega_0 - l\omega_s)\tau} \cdot \\ & G_{k-lN} H(k\omega_0 - l\omega_s + 2\pi\nu). \end{aligned} \tag{28}$$

Here $L_n(k)$ and $L_p(k)$ denote the number of spectrum points in the negative, and positive frequency domain that superpose at the frequency point $k\omega_0$. These limits are given by

$$L_n(k) = \left\lfloor \frac{\frac{K}{2}+k}{N} \right\rfloor, \tag{29}$$

$$L_p(k) = \left\lfloor \frac{\frac{K}{2}-1-k}{N} \right\rfloor. \tag{30}$$

For simplicity, we restrict the transmit bandwidth B to be a multiple of the sampling frequency $\omega_s = 2\pi f_s$, i.e,

$$2\pi B = 2L\omega_s + N\omega_0 = (2L+1)\,\omega_s, \quad L \in \mathbb{N}_0, \tag{31}$$

which results in

$$L_n(k) = L_p(k) = L. \tag{32}$$

Note that in the following this restriction leads to a compact notation for the EFIM. The extension to the case with arbitrary bandwidth B is always possible by using the expressions (29), (30). Stacking the entries (28) into a vector yields

$$\boldsymbol{v}(\boldsymbol{\theta}) = \gamma\sqrt{N} \boldsymbol{\Delta}(\nu) \boldsymbol{W}^{\mathrm{H}} \boldsymbol{A} \boldsymbol{T}(\tau) \big(\tilde{\boldsymbol{g}} \circ \tilde{\boldsymbol{h}}(\nu) \big). \tag{33}$$

Denoting $\boldsymbol{I}_N$ as the identity matrix of size N and $\circ$ as the element-wise Hadamard product, (33) contains an aliasing matrix

$$\boldsymbol{A} = [\boldsymbol{I}_N, \ldots, \boldsymbol{I}_N] \in \mathbb{R}^{N\times K}, \tag{34}$$

a diagonal time-delay matrix $\boldsymbol{T}(\tau) \in \mathbb{C}^{K\times K}$ with entries

$$[\boldsymbol{T}(\tau)]_{ii} = \mathrm{e}^{-\mathrm{j}\left(i-\frac{K}{2}-1\right)\omega_0\tau}, \tag{35}$$

and the transmit filter spectrum vector $\tilde{\boldsymbol{g}} \in \mathbb{C}^K$ with elements

$$[\tilde{\boldsymbol{g}}]_i = G_{i-\frac{K}{2}-1}. \tag{36}$$

Throughout this work vector and matrix entries are referenced by positive integers, starting at 1 and therefore $i \in \{1, 2, \ldots, K\}$ for both preceding equations. The vector $\tilde{\boldsymbol{h}}(\nu) \in \mathbb{C}^K$ in (33) denotes the frequency shifted receive filter spectrum with entries

$$[\tilde{\boldsymbol{h}}(\nu)]_i = H\left(\left(i - \frac{K}{2} - 1 \right) \omega_0 + 2\pi\nu \right). \tag{37}$$

Further, in (33) $\boldsymbol{W} \in \mathbb{C}^{N\times N}$ is the DFT matrix

$$[\boldsymbol{W}]_{ij} = \frac{1}{\sqrt{N}} \mathrm{e}^{-\mathrm{j}2\pi \frac{\left(i-\frac{N}{2}-1\right)\left(j-\frac{N}{2}-1\right)}{N}}, \tag{38}$$

where $i, j \in \{1, 2, \ldots, N\}$ and $\boldsymbol{\Delta}(\nu) \in \mathbb{C}^{N\times N}$ represents the diagonal matrix

$$[\boldsymbol{\Delta}(\nu)]_{ii} = \mathrm{e}^{\mathrm{j}2\pi\left(i-\frac{N}{2}-1\right)\nu T_s}. \tag{39}$$

Introducing the Doppler convolution matrix

$$\tilde{\boldsymbol{\Delta}}(\nu) = \boldsymbol{W} \boldsymbol{\Delta}(\nu) \boldsymbol{W}^{\mathrm{H}} \in \mathbb{C}^{N\times N}, \tag{40}$$

a signal representation in the frequency domain

$$\begin{aligned} \boldsymbol{v}(\boldsymbol{\theta}) &= \gamma\sqrt{N} \boldsymbol{W}^{\mathrm{H}} \tilde{\boldsymbol{\Delta}}(\nu) \boldsymbol{A} \boldsymbol{T}(\tau) \big(\tilde{\boldsymbol{g}} \circ \tilde{\boldsymbol{h}}(\nu) \big) \\ &= \sqrt{N} \boldsymbol{W}^{\mathrm{H}} \tilde{\boldsymbol{v}}(\boldsymbol{\theta}) \end{aligned} \tag{41}$$

is obtained from (33), where

$$\tilde{\boldsymbol{v}}(\boldsymbol{\theta}) = \gamma \tilde{\boldsymbol{\Delta}}(\nu) \boldsymbol{A} \boldsymbol{T}(\tau) \big(\tilde{\boldsymbol{g}} \circ \tilde{\boldsymbol{h}}(\nu) \big) \tag{42}$$

is the attenuated and delay-Doppler shifted receive signal spectrum. A frequency domain representation of the noise covariance matrix (7) is obtained by the transformation

$$\tilde{\boldsymbol{R}}_{\boldsymbol{\eta}} = \boldsymbol{W} \boldsymbol{R}_{\boldsymbol{\eta}} \boldsymbol{W}^{\mathrm{H}}. \tag{43}$$

Note that due to the Doppler shift in (37), frequencies $k\omega_0 + 2\pi\nu$ of the receive filter $H(\omega)$ have to be considered for evaluation of the filtered and sampled signal $\boldsymbol{v}(\boldsymbol{\theta})$. The entries of the FIM $\boldsymbol{J}(\boldsymbol{\theta})$ are directly obtained by plugging (41) into (13) and can be found in [8].

VI. Approximation of the Delay-Doppler FIM

The expressions for the FIM make it possible to formulate the transceiver optimization problem (18) for the delay-Doppler channel model (19). Due to the assumption of a periodic transmit sequence $\breve{x}(t)$, the minimization over the transmit filter $g(t)$ reduces to an optimization with respect to the K entries of $\tilde{\boldsymbol{g}}$. However, due to its dependence on the Doppler shift ν, optimization of the receive filter $h(t)$ requires one to solve a maximization problem over an infinite number of variables forming $\tilde{\boldsymbol{h}}(\nu)$. Therefore in the following section we discuss several steps to approximate the FIM entries and formulate a tractable optimization problem (18).

A. FIM Approximation - Periodic Doppler

In order to tackle the problem of optimizing over an uncountable set of receive filter variables $\tilde{\boldsymbol{h}}_d(\nu)$, we approximate the Doppler shift to be periodic with T_0, i.e.,

$$\mathrm{e}^{\mathrm{j}2\pi\nu t} \approx \mathrm{e}^{\mathrm{j}2\pi\nu(t \operatorname{modc} T_0)}, \tag{44}$$

where we use a centered version of the modulo operation

$$t \operatorname{modc} T_0 = \left(\left(t + \frac{T_0}{2}\right) \bmod T_0\right) - \frac{T_0}{2}. \tag{45}$$

Note that in the interval $t \in \left[-\frac{T_0}{2}, \frac{T_0}{2}\right)$ the approximation (44) is exact. However, due to the filtering operation $h(t)$ portions of the signal outside that time range are convolved into the sampling interval and thus produce an approximation error.

Under the assumption (44), it is possible to write

$$\mathrm{e}^{\mathrm{j}2\pi\nu(t \operatorname{modc} T_0)} = \sum_{z=-\infty}^{\infty} d_z(\nu)\mathrm{e}^{\mathrm{j}z\omega_0 t}. \tag{46}$$

Calculating the Fourier coefficients $d_z(\nu)$ yields

$$d_z(\nu) = \begin{cases} \frac{\sin(\pi T_0\nu - \pi z)}{\pi T_0\nu - \pi z}, & z \neq T_0\nu \\ 1, & z = T_0\nu \end{cases}. \tag{47}$$

Replacing the Doppler shift in (19) with the approximation (44) yields the signal approximation $\bar{v}(t;\boldsymbol{\theta})$, that evaluates to

$$\begin{aligned}\bar{v}(t;\boldsymbol{\theta}) &= \gamma \sum_{k\in\mathcal{K}} \sum_{z=-\infty}^{\infty} G_k d_z(\nu)\mathrm{e}^{-\mathrm{j}k\omega_0\tau}\mathrm{e}^{\mathrm{j}(k+z)\omega_0 t} * h(t) \\ &= \gamma \sum_{k\in\mathcal{K}} \sum_{z=-\infty}^{\infty} G_k d_z(\nu)\mathrm{e}^{-\mathrm{j}k\omega_0\tau}\mathrm{e}^{\mathrm{j}(k+z)\omega_0 t} H\big((k+z)\omega_0\big) \\ &= \gamma \sum_{k\in\mathcal{K}} \sum_{m=-\infty}^{\infty} G_k d_{m-k}(\nu)\mathrm{e}^{-\mathrm{j}k\omega_0\tau}\mathrm{e}^{\mathrm{j}m\omega_0 t} H(m\omega_0), \end{aligned} \tag{48}$$

with the substitution $z = m - k$. Using the abbreviation

$$H_m = H(m\omega_0), \tag{49}$$

the signal samples are given by

$$\begin{aligned}\bar{v}(nT_s;\boldsymbol{\theta}) &= \gamma \sum_{m=-\infty}^{\infty} \mathrm{e}^{\mathrm{j}2\pi\frac{mn}{N}} H_m \sum_{k\in\mathcal{K}} G_k d_{m-k}(\nu)\mathrm{e}^{-\mathrm{j}k\omega_0\tau} \\ &= \gamma \sum_{m=-\frac{N}{2}}^{\frac{N}{2}-1} \mathrm{e}^{\mathrm{j}2\pi\frac{mn}{N}} \sum_{l=-\infty}^{\infty} H_{m-lN} \\ &\quad \sum_{k\in\mathcal{K}} G_k d_{m-lN-k}(\nu)\mathrm{e}^{-\mathrm{j}k\omega_0\tau}. \end{aligned} \tag{50}$$

Neither the time-delay nor the Doppler shift have a significant impact on the signal bandwidth B and thus the receive filter can also be assumed to have bandwidth B. Therefore,

$$\begin{aligned}\bar{v}(nT_s;\boldsymbol{\theta}) = \gamma \sum_{m=-\frac{N}{2}}^{\frac{N}{2}-1} \mathrm{e}^{\mathrm{j}2\pi\frac{mn}{N}} \sum_{l=-L}^{L} H\Big((m-lN)\omega_0\Big) \cdot \\ \sum_{k\in\mathcal{K}} G_k d_{m-lN-k}(\nu)\mathrm{e}^{-\mathrm{j}k\omega_0\tau}. \end{aligned} \tag{51}$$

In vector notation, we obtain

$$\begin{aligned}\bar{\boldsymbol{v}}(\boldsymbol{\theta}) &\approx \sqrt{N}\gamma \boldsymbol{W}^{\mathrm{H}} \boldsymbol{A}\big(\tilde{\boldsymbol{h}} \circ \boldsymbol{D}(\nu)\boldsymbol{T}(\tau)\tilde{\boldsymbol{g}}\big) \\ &= \sqrt{N}\boldsymbol{W}^{\mathrm{H}}\tilde{\bar{\boldsymbol{v}}}(\boldsymbol{\theta}), \end{aligned} \tag{52}$$

where the approximated receive pilot spectrum is

$$\tilde{\bar{\boldsymbol{v}}}(\boldsymbol{\theta}) = \gamma \boldsymbol{A}(\tilde{\boldsymbol{h}} \circ \boldsymbol{D}(\nu)\boldsymbol{T}(\tau)\tilde{\boldsymbol{g}}), \tag{53}$$

with the Doppler convolution matrix

$$\boldsymbol{D}(\nu) = \begin{pmatrix} d_0(\nu) & d_{-1}(\nu) & \dots & d_{-K+1}(\nu) \\ d_1(\nu) & d_0(\nu) & \dots & d_{-K+2}(\nu) \\ \vdots & \vdots & \ddots & \vdots \\ d_{K-1}(\nu) & d_{K-2}(\nu) & \dots & d_0(\nu) \end{pmatrix} \in \mathbb{C}^{K\times K} \tag{54}$$

and the receive filter spectrum $\tilde{\boldsymbol{h}} \in \mathbb{C}^K$

$$[\tilde{\boldsymbol{h}}]_i = H\left(\Big(i - \frac{K}{2} - 1\Big)\omega_0\right). \tag{55}$$

The advantage of the periodic Doppler approximation (44) stems from the fact that the filter spectrum $\tilde{\boldsymbol{h}}$ does not depend on the Doppler ν. This implies that due to the periodicity of $\bar{v}(t;\boldsymbol{\theta})$ only the harmonics $k\omega_0$ of the receive filter $H(\omega)$ are excited and other parts of the filter spectrum do not impact the description of the received signal. Defining the channel matrix

$$\boldsymbol{C}(\boldsymbol{\theta}) = \gamma \boldsymbol{D}(\nu)\boldsymbol{T}(\tau), \tag{56}$$

the receive signal spectrum can be represented by

$$\tilde{\bar{\boldsymbol{v}}}(\boldsymbol{\theta}) = \boldsymbol{A}\big(\tilde{\boldsymbol{h}} \circ \boldsymbol{C}(\boldsymbol{\theta})\tilde{\boldsymbol{g}}\big). \tag{57}$$

B. FIM Approximation - Circular Noise Covariance

Computation of the FIM entries (13) requires the inverse of the noise covariance matrix $\boldsymbol{R}_{\boldsymbol{\eta}}^{-1}$. The fact that $\boldsymbol{R}_{\boldsymbol{\eta}}$ is a non-trivial function of the receive filter $h(t)$ hinders tackling the optimization problem (18). We exploit the fact that in the large sample regime, the noise covariance $\boldsymbol{R}_{\boldsymbol{\eta}}$ is approximately diagonalized by the DFT matrix, i.e.,

$$\boldsymbol{\Omega}_{\boldsymbol{\eta}} \approx \boldsymbol{W}\boldsymbol{R}_{\boldsymbol{\eta}}\boldsymbol{W}^{\mathrm{H}}, \tag{58}$$

where $\boldsymbol{\Omega}_{\boldsymbol{\eta}} \in \mathbb{R}^{N\times N}$ is a diagonal matrix with entries

$$[\boldsymbol{\Omega}_{\boldsymbol{\eta}}]_{ii} = \frac{1}{T_s} \sum_{l=-L}^{L} \left| H\left(\left(i - \frac{N}{2} - 1\right)\omega_0 - l\omega_s\right)\right|^2. \tag{59}$$

Note that (58) results from Szegös theorem [48] applied to Toeplitz matrices. Defining the receive filter spectrum matrix

$$\boldsymbol{H} = \operatorname{diag}(\tilde{\boldsymbol{h}}) \in \mathbb{C}^{K\times K}, \tag{60}$$

we directly find the useful expression

$$\boldsymbol{\Omega}_{\boldsymbol{\eta}} = \frac{1}{T_s}\boldsymbol{A}\boldsymbol{H}\boldsymbol{H}^{\mathrm{H}}\boldsymbol{A}^{\mathrm{H}}. \tag{61}$$

C. Approximated FIM Entries

With the approximations (44) and (58), the FIM elements (12) are directly obtained by inserting (52) and (58) into (13)

$$[\bar{\boldsymbol{J}}_F(\boldsymbol{\theta})]_{ij} = 2\mathrm{Re}\left\{ N \frac{\partial \tilde{\bar{\boldsymbol{v}}}^{\mathrm{H}}(\boldsymbol{\theta})}{\partial [\boldsymbol{\theta}]_i} \boldsymbol{\Omega}_{\boldsymbol{\eta}}^{-1} \frac{\partial \tilde{\bar{\boldsymbol{v}}}(\boldsymbol{\theta})}{\partial [\boldsymbol{\theta}]_j} \right\} = \\ = 2N\mathrm{Re}\left\{ \left(\tilde{\boldsymbol{h}} \circ \frac{\partial \boldsymbol{C}(\boldsymbol{\theta})}{\partial [\boldsymbol{\theta}]_i} \tilde{\boldsymbol{g}} \right)^{\mathrm{H}} \boldsymbol{A}^{\mathrm{H}} \boldsymbol{\Omega}_{\boldsymbol{\eta}}^{-1} \boldsymbol{A} \left(\tilde{\boldsymbol{h}} \circ \frac{\partial \boldsymbol{C}(\boldsymbol{\theta})}{\partial [\boldsymbol{\theta}]_j} \tilde{\boldsymbol{g}} \right) \right\}, \tag{62}$$

where $\bar{\boldsymbol{J}}_F(\boldsymbol{\theta})$ denotes the FIM that stems from the periodic Doppler and noise covariance approximation. Using the diagonalization property for the Hadamard product of two vectors, equation (62) can be denoted by

$$[\bar{\boldsymbol{J}}_F(\boldsymbol{\theta})]_{ij} = \tilde{\boldsymbol{g}}^{\mathrm{H}} \big(\boldsymbol{\Phi}_{ij}(\boldsymbol{\theta}) + \boldsymbol{\Phi}_{ji}(\boldsymbol{\theta}) \big) \tilde{\boldsymbol{g}}, \tag{63}$$

with

$$\boldsymbol{\Phi}_{ij}(\boldsymbol{\theta}) = N \frac{\partial \boldsymbol{C}^{\mathrm{H}}(\boldsymbol{\theta})}{\partial [\boldsymbol{\theta}]_i} \boldsymbol{H}^{\mathrm{H}} \boldsymbol{A}^{\mathrm{H}} \boldsymbol{\Omega}_{\boldsymbol{\eta}}^{-1} \boldsymbol{A} \boldsymbol{H} \frac{\partial \boldsymbol{C}(\boldsymbol{\theta})}{\partial [\boldsymbol{\theta}]_j} \in \mathbb{C}^{K \times K}. \tag{64}$$

The FIM expression (63) allows us to approximate the objective function (18) by

$$\begin{aligned} \mathrm{tr}(\boldsymbol{M}' \boldsymbol{J}_D) \approx \mathrm{tr}(\boldsymbol{M}' \bar{\boldsymbol{J}}_D) &= \sum_{i=1}^{2} \sum_{j=1}^{2} [\boldsymbol{M}']_{ji} [\bar{\boldsymbol{J}}_D]_{ij} \\ &= \sum_{i=1}^{2} \sum_{j=1}^{2} [\boldsymbol{M}']_{ji} \mathrm{E}_{\boldsymbol{\theta}} \left\{ [\bar{\boldsymbol{J}}_F(\boldsymbol{\theta})]_{ij} \right\} \\ &= \tilde{\boldsymbol{g}}^{\mathrm{H}} \boldsymbol{\Phi} \tilde{\boldsymbol{g}}, \end{aligned} \tag{65}$$

with

$$\boldsymbol{\Phi} = \sum_{i=1}^{2} \sum_{j=1}^{2} [\boldsymbol{M}']_{ji} \mathrm{E}_{\boldsymbol{\theta}} \left[\boldsymbol{\Phi}_{ij}(\boldsymbol{\theta}) + \boldsymbol{\Phi}_{ji}(\boldsymbol{\theta}) \right]. \tag{66}$$

Alternatively to (63), it is possible to emphasize the dependence of the FIM on $\tilde{\boldsymbol{h}}$ and reformulate (62) as

$$[\bar{\boldsymbol{J}}_F(\boldsymbol{\theta})]_{ij} = 2\mathrm{Re}\left\{ \big(\boldsymbol{A}(\boldsymbol{\xi}_i(\boldsymbol{\theta}) \circ \tilde{\boldsymbol{h}}) \big)^{\mathrm{H}} \boldsymbol{\Omega}_{\boldsymbol{\eta}}^{-1} \boldsymbol{A}(\boldsymbol{\xi}_j(\boldsymbol{\theta}) \circ \tilde{\boldsymbol{h}}) \right\}, \tag{67}$$

where

$$\boldsymbol{\xi}_i(\boldsymbol{\theta}) = \sqrt{N} \frac{\partial \boldsymbol{C}(\boldsymbol{\theta})}{\partial [\boldsymbol{\theta}]_i} \tilde{\boldsymbol{g}}. \tag{68}$$

The filter spectrum points

$$\tilde{\boldsymbol{h}}_k = [H_{k-lN}, H_{k-(l-1)N}, \dots H_{k+lN}]^{\mathrm{T}}, \tag{69}$$

separated by ω_s, experience aliasing since they are combined by the multiplication of $\boldsymbol{\xi}_i(\boldsymbol{\theta}) \circ \tilde{\boldsymbol{h}}$ with $\boldsymbol{A}$, where the corresponding coefficients are

$$[\boldsymbol{\xi}_{k,i}(\boldsymbol{\theta})]_l = [\boldsymbol{\xi}_i(\boldsymbol{\theta})]_{k-lN+\frac{K}{2}+1}. \tag{70}$$

Thus, the compact FIM representation

$$[\bar{\boldsymbol{J}}_F(\boldsymbol{\theta})]_{ij} = 2\mathrm{Re}\left\{ \sum_{k=-\frac{N}{2}}^{\frac{N}{2}-1} \frac{\tilde{\boldsymbol{h}}_k^{\mathrm{H}} \boldsymbol{\xi}_{k,i}^*(\boldsymbol{\theta}) \boldsymbol{\xi}_{k,j}^{\mathrm{T}}(\boldsymbol{\theta}) \tilde{\boldsymbol{h}}_k}{\tilde{\boldsymbol{h}}_k^{\mathrm{H}} \tilde{\boldsymbol{h}}_k} \right\} \tag{71}$$

is obtained. Note that in (70) the summand $\frac{K}{2}+1$ assures a correct indexing of the vector $\boldsymbol{\xi}_i(\boldsymbol{\theta})$. In contrast to (65), eq. (71) allows us to characterize the objective function

$$\mathrm{tr}(\boldsymbol{M}' \bar{\boldsymbol{J}}_D) = \sum_{k \in \mathcal{N}} \frac{\tilde{\boldsymbol{h}}_k^{\mathrm{H}} \boldsymbol{\Delta}_k \tilde{\boldsymbol{h}}_k}{\tilde{\boldsymbol{h}}_k^{\mathrm{H}} \tilde{\boldsymbol{h}}_k}, \tag{72}$$

with

$$\boldsymbol{\Delta}_k = \sum_{i=1}^{2} \sum_{j=1}^{2} [\boldsymbol{M}']_{ji} \mathrm{E}_{\boldsymbol{\theta}} \left[\boldsymbol{\xi}_{k,i}^* \boldsymbol{\xi}_{k,j}^{\mathrm{T}} + \boldsymbol{\xi}_{k,j}^* \boldsymbol{\xi}_{k,i}^{\mathrm{T}} \right]. \tag{73}$$

Note that (65) emphasizes the quadratic dependence of the cost function $\mathrm{tr}(\boldsymbol{M}' \bar{\boldsymbol{J}}_D)$ on the transmit spectrum $\tilde{\boldsymbol{g}}$, while (72) is written as a function of the receive filter $\tilde{\boldsymbol{h}}$.

VII. Symmetry of the EFIM

The EFIM exhibits a symmetry with respect to time and frequency reversal of the two filters $\tilde{\boldsymbol{g}}$ and $\tilde{\boldsymbol{h}}$. We will see later that this observation can be used to accelerate the optimization algorithm solving the transceiver design problem (18).

A. EFIM with Mirrored Transceive Filter Spectra

Define the mirroring matrix

$$\boldsymbol{\Pi} = \begin{bmatrix} 0 & \dots & 0 & 1 \\ \vdots & \iddots & 1 & 0 \\ 0 & \iddots & \iddots & \vdots \\ 1 & 0 & \dots & 0 \end{bmatrix} \in \mathbb{R}^{K \times K}, \tag{74}$$

which obeys

$$\boldsymbol{\Pi}^{\mathrm{H}} = \boldsymbol{\Pi}^{-1} = \boldsymbol{\Pi}, \tag{75}$$

such that the frequency mirroring operations $X(-\omega)$ and $H(-\omega)$ can be denoted as $\boldsymbol{\Pi}\tilde{\boldsymbol{g}}$ and $\boldsymbol{\Pi}\boldsymbol{H}\boldsymbol{\Pi}$, respectively. Writing $\bar{\boldsymbol{J}}_F(\boldsymbol{\theta})\big|_{\tilde{\boldsymbol{g}},\tilde{\boldsymbol{h}}}$ to denote the FIM with transmit $\tilde{\boldsymbol{g}}$ and receive filter spectrum $\tilde{\boldsymbol{h}}$, we find the FIM entries after mirroring the transceive filters along the frequency axis

$$\begin{aligned} \left[\bar{\boldsymbol{J}}_F(\boldsymbol{\theta})\big|_{\boldsymbol{\Pi}\tilde{\boldsymbol{g}},\boldsymbol{\Pi}\tilde{\boldsymbol{h}}} \right]_{ij} = 2N\mathrm{Re}\Bigg\{ & \tilde{\boldsymbol{g}}^{\mathrm{H}} \boldsymbol{\Pi} \frac{\partial \boldsymbol{C}^{\mathrm{H}}(\boldsymbol{\theta})}{\partial [\boldsymbol{\theta}]_i} \boldsymbol{\Pi} \boldsymbol{H}^{\mathrm{H}} \boldsymbol{\Pi} \boldsymbol{A}^{\mathrm{H}} \boldsymbol{\Pi} \boldsymbol{\Omega}_{\boldsymbol{\eta}}^{-1} \cdot \\ & \boldsymbol{\Pi} \boldsymbol{A} \boldsymbol{\Pi} \boldsymbol{H} \boldsymbol{\Pi} \frac{\partial \boldsymbol{C}(\boldsymbol{\theta})}{\partial [\boldsymbol{\theta}]_j} \boldsymbol{\Pi} \tilde{\boldsymbol{g}} \Bigg\} \\ = 2N\mathrm{Re}\Bigg\{ & \tilde{\boldsymbol{g}}^{\mathrm{H}} \boldsymbol{\Pi} \frac{\partial \boldsymbol{C}^{\mathrm{H}}(\boldsymbol{\theta})}{\partial [\boldsymbol{\theta}]_i} \boldsymbol{\Pi} \boldsymbol{H}^{\mathrm{H}} \boldsymbol{A}^{\mathrm{H}} \boldsymbol{\Omega}_{\boldsymbol{\eta}}^{-1} \boldsymbol{A} \boldsymbol{H} \boldsymbol{\Pi} \frac{\partial \boldsymbol{C}(\boldsymbol{\theta})}{\partial [\boldsymbol{\theta}]_j} \boldsymbol{\Pi} \tilde{\boldsymbol{g}} \Bigg\}. \end{aligned} \tag{76}$$

It can be seen that (76) contains the mirrored channel matrix

$$\begin{aligned} \boldsymbol{\Pi} \frac{\partial \boldsymbol{C}(\boldsymbol{\theta})}{\partial [\boldsymbol{\theta}]_i} \boldsymbol{\Pi} &= \frac{\partial}{\partial [\boldsymbol{\theta}]_i} \left(\gamma \boldsymbol{\Pi} \boldsymbol{D}(\nu) \boldsymbol{T}(\tau) \boldsymbol{\Pi} \right) \\ &= \frac{\partial}{\partial [\boldsymbol{\theta}]_i} \left(\gamma \boldsymbol{\Pi} \boldsymbol{D}(\nu) \boldsymbol{\Pi} \boldsymbol{\Pi} \boldsymbol{T}(\tau) \boldsymbol{\Pi} \right). \end{aligned} \tag{77}$$

With the structure of the time-delay matrix (35), we have

$$\boldsymbol{\Pi} \boldsymbol{T}(\tau) \boldsymbol{\Pi} \approx \boldsymbol{T}(-\tau), \tag{78}$$

and with the equality

$$d_{-z}(\nu) = \frac{\sin(\pi T_0 \nu + \pi z)}{\pi T_0 \nu + \pi z} = d_z(-\nu), \tag{79}$$

we obtain

$$\boldsymbol{\Pi} \boldsymbol{D}(\nu) \boldsymbol{\Pi} = \boldsymbol{D}(-\nu). \tag{80}$$

Thus,

$$\boldsymbol{\Pi} \frac{\partial \boldsymbol{C}(\boldsymbol{\theta})}{\partial [\boldsymbol{\theta}]_i} \boldsymbol{\Pi} \approx \frac{\partial}{\partial [\boldsymbol{\theta}]_i} \boldsymbol{C}(-\boldsymbol{\theta}) = - \frac{\partial \boldsymbol{C}(\boldsymbol{\theta}')}{\partial [\boldsymbol{\theta}']_i} \bigg|_{\boldsymbol{\theta}' = -\boldsymbol{\theta}}, \tag{81}$$

showing that applying the mirroring operation to both filters corresponds to a reversal of the channel parameters, i.e.,

$$\Big[\bar{\boldsymbol{J}}_F(\boldsymbol{\theta}) \big|_{\boldsymbol{\Pi}\tilde{\boldsymbol{g}}, \boldsymbol{\Pi}\tilde{\boldsymbol{h}}} \Big]_{ij} \approx \Big[\bar{\boldsymbol{J}}_F(-\boldsymbol{\theta}) \big|_{\tilde{\boldsymbol{g}}, \tilde{\boldsymbol{h}}} \Big]_{ij}. \tag{82}$$

The time-delay and Doppler shift are assumed to be normally distributed and thus have symmetric distributions, i.e.,

$$p(\boldsymbol{\theta}) = p(-\boldsymbol{\theta}). \tag{83}$$

In general, mirroring a function when averaging with respect to a symmetric distribution does not influence the expected value and thus we obtain the approximate identity

$$\bar{\boldsymbol{J}}_D |_{\tilde{\boldsymbol{g}}, \tilde{\boldsymbol{h}}} \approx \bar{\boldsymbol{J}}_D |_{\boldsymbol{\Pi}\tilde{\boldsymbol{g}}, \boldsymbol{\Pi}\tilde{\boldsymbol{h}}}. \tag{84}$$

Note, that using the properties of the Fourier transform, the same result is obtained when mirroring the transmit signal and receive signal in the time domain.

B. Off-Diagonal Elements of the EFIM with Symmetric Filters

We will show in the following that for symmetric transceiver filters the non-diagonal elements of the FIM vanish. Due to the symmetry and by the properties of the Fourier transform, $\tilde{\boldsymbol{g}}, \tilde{\boldsymbol{h}}$ become real-valued. Therefore, we have

$$\begin{aligned} \big[\bar{\boldsymbol{J}}_F(\boldsymbol{\theta}) \big]_{ij} &= 2\mathrm{Re} \Big\{ \tilde{\boldsymbol{g}}^{\mathrm{H}} \boldsymbol{\Phi}_{ij}(\boldsymbol{\theta}) \tilde{\boldsymbol{g}} \Big\} \\ &= \tilde{\boldsymbol{g}}^{\mathrm{H}} \boldsymbol{\Phi}_{ij}(\boldsymbol{\theta}) \tilde{\boldsymbol{g}} + \tilde{\boldsymbol{g}}^{\mathrm{T}} \boldsymbol{\Phi}_{ij}^*(\boldsymbol{\theta}) \tilde{\boldsymbol{g}}^* \\ &= \tilde{\boldsymbol{g}}^{\mathrm{H}} \big(\boldsymbol{\Phi}_{ij}(\boldsymbol{\theta}) + \boldsymbol{\Phi}_{ij}^*(\boldsymbol{\theta}) \big) \tilde{\boldsymbol{g}}. \end{aligned} \tag{85}$$

It is straightforward to show that the following properties hold for the complex conjugates

$$\boldsymbol{T}^*(\tau) = \boldsymbol{T}(-\tau), \tag{86}$$

$$\boldsymbol{D}^*(\nu) = \boldsymbol{D}(\nu). \tag{87}$$

For the off-diagonal elements of the FIM, the matrices $\boldsymbol{\Phi}_{ij}(\boldsymbol{\theta})$ contain exactly one partial derivative with respect to τ and one with respect to ν. Hence, for $i \neq j$

$$\big[\bar{\boldsymbol{J}}_F(\boldsymbol{\theta}) \big]_{ij} = \tilde{\boldsymbol{g}}^{\mathrm{H}} \big(\boldsymbol{\Phi}_{ij}(\tau, \nu) - \boldsymbol{\Phi}_{ij}(-\tau, \nu) \big) \tilde{\boldsymbol{g}}. \tag{88}$$

Due to the assumed symmetry of the distribution of the time-delay $p(\tau) = p(-\tau)$, taking the expected value of (88), the off-diagonal elements of the EFIM $\bar{\boldsymbol{J}}_D$ become

$$[\bar{\boldsymbol{J}}_D]_{12} = [\bar{\boldsymbol{J}}_D]_{21} = 0. \tag{89}$$

C. Compact Cost Functions

With (84), the reversal of the transmit and the receive filter in the frequency domain does not significantly change the elements of the EFIM if the parameters are distributed symmetrically. Motivated by this observation, we will solve the optimization problem (18) under the assumption of symmetric receive and transmit filters and thus, we restrict the transceive filters $\tilde{\boldsymbol{g}}$ and $\tilde{\boldsymbol{h}}$ to have symmetric impulse responses and spectra. Consequently, due the properties of the Fourier transform, both filters are real-valued. Under this assumption, optimization over only one half of the spectrum is required.

We split the transmit signal

$$\tilde{\boldsymbol{g}} = \begin{bmatrix} 0 & \tilde{\boldsymbol{g}}_{\mathrm{r}}^{\mathrm{T}} & \tilde{g}_0 & \tilde{\boldsymbol{g}}_{\mathrm{f,r}}^{\mathrm{T}} \end{bmatrix}^{\mathrm{T}}, \tag{90}$$

with the one-sided transmit spectrum $\tilde{\boldsymbol{g}}_{\mathrm{r}} \in \mathbb{R}^{\frac{K}{2}-1}$ and $\tilde{\boldsymbol{g}}_{\mathrm{f,r}} = \boldsymbol{\Pi}\tilde{\boldsymbol{g}}_{\mathrm{r}}$. Note that the first element in (90) has been set to zero, i.e., $G_{-\frac{K}{2}} = 0$, in order to obtain a fully symmetric description. This allows us to rewrite the cost function (65) as

$$\begin{aligned} \tilde{\boldsymbol{g}}^{\mathrm{H}} \boldsymbol{\Phi} \tilde{\boldsymbol{g}} &= \begin{bmatrix} 0 & \tilde{\boldsymbol{g}}_{\mathrm{r}}^{\mathrm{T}} & \tilde{g}_0 & \tilde{\boldsymbol{g}}_{\mathrm{f,r}}^{\mathrm{T}} \end{bmatrix} \boldsymbol{\phi} \begin{bmatrix} 0 \\ \tilde{\boldsymbol{g}}_{\mathrm{r}} \\ \tilde{g}_0 \\ \tilde{\boldsymbol{g}}_{\mathrm{f,r}} \end{bmatrix} \\ &= \begin{bmatrix} \tilde{\boldsymbol{g}}_{\mathrm{r}}^{\mathrm{T}} & \tilde{g}_0 & \tilde{\boldsymbol{g}}_{\mathrm{f,r}}^{\mathrm{T}} \end{bmatrix} \begin{bmatrix} \boldsymbol{\phi}_{11} & \boldsymbol{\phi}_2 & \boldsymbol{\phi}_{12} \\ \boldsymbol{\phi}_1^{\mathrm{T}} & \phi_0 & \boldsymbol{\phi}_3^{\mathrm{T}} \\ \boldsymbol{\phi}_{21} & \boldsymbol{\phi}_4 & \boldsymbol{\phi}_{22} \end{bmatrix} \begin{bmatrix} \tilde{\boldsymbol{g}}_{\mathrm{r}} \\ \tilde{g}_0 \\ \tilde{\boldsymbol{g}}_{\mathrm{f,r}} \end{bmatrix} \\ &= \begin{bmatrix} \tilde{\boldsymbol{g}}_{\mathrm{r}}^{\mathrm{T}} & \tilde{g}_0 \end{bmatrix} \begin{bmatrix} \boldsymbol{\phi}_r & \boldsymbol{\phi}_2 + \boldsymbol{\Pi}\boldsymbol{\phi}_4 \\ (\boldsymbol{\phi}_1 + \boldsymbol{\Pi}\boldsymbol{\phi}_3)^{\mathrm{T}} & \phi_0 \end{bmatrix} \begin{bmatrix} \tilde{\boldsymbol{g}}_{\mathrm{r}} \\ \tilde{g}_0 \end{bmatrix}, \end{aligned} \tag{91}$$

with the matrices and vectors

$$\boldsymbol{\phi}_{11}, \boldsymbol{\phi}_{12}, \boldsymbol{\phi}_{21}, \boldsymbol{\phi}_{22} \in \mathbb{C}^{\left(\frac{K}{2}-1\right) \times \left(\frac{K}{2}-1\right)}, \tag{92}$$

$$\boldsymbol{\phi}_1, \boldsymbol{\phi}_2, \boldsymbol{\phi}_3, \boldsymbol{\phi}_4 \in \mathbb{C}^{\frac{K}{2}-1} \tag{93}$$

and a reduced filter matrix

$$\boldsymbol{\phi}_{\mathrm{r}} = \boldsymbol{\phi}_{11} + \boldsymbol{\phi}_{12}\boldsymbol{\Pi} + \boldsymbol{\Pi}\boldsymbol{\phi}_{21} + \boldsymbol{\Pi}\boldsymbol{\phi}_{22}\boldsymbol{\Pi}. \tag{94}$$

It can be seen that with symmetric filters the cost function (65) can be written in a compact quadratic form (91), requiring only one side of the transmit filter spectrum $\tilde{\boldsymbol{g}}$. A compact version of (72) can be found in a similar way

$$\tilde{\boldsymbol{h}}_k = \boldsymbol{\Pi}\tilde{\boldsymbol{h}}_{-k}. \tag{95}$$

This allows to rewrite the cost function (72) as

$$\begin{aligned} \sum_{k=-\frac{N}{2}}^{\frac{N}{2}-1} \frac{\tilde{\boldsymbol{h}}_k^{\mathrm{H}} \boldsymbol{\Delta}_k \tilde{\boldsymbol{h}}_k}{\tilde{\boldsymbol{h}}_k^{\mathrm{H}} \tilde{\boldsymbol{h}}_k} &= \sum_{k=-\frac{N}{2}+1}^{-1} \frac{\tilde{\boldsymbol{h}}_k^{\mathrm{H}} (\boldsymbol{\Delta}_k + \boldsymbol{\Pi}\boldsymbol{\Delta}_{-k}\boldsymbol{\Pi}) \tilde{\boldsymbol{h}}_k}{\tilde{\boldsymbol{h}}_k^{\mathrm{H}} \tilde{\boldsymbol{h}}_k} \\ &\quad + \sum_{k \in \left\{-\frac{N}{2}, 0\right\}} \frac{\tilde{\boldsymbol{h}}_k^{\mathrm{H}} \boldsymbol{\Delta}_k \tilde{\boldsymbol{h}}_k}{\tilde{\boldsymbol{h}}_k^{\mathrm{H}} \tilde{\boldsymbol{h}}_k}. \end{aligned} \tag{96}$$

VIII. Transceiver Optimization Algorithm

In the following we focus on solving the transceiver design problem (18) with the simplifications of the FIM derived in

the previous section. With the frequency domain representation (36) and (55), the optimization problem (18) can be stated as

$$\max_{\tilde{\boldsymbol{g}},\tilde{\boldsymbol{h}}} \quad \mathrm{tr}\left(\boldsymbol{M}'\bar{\boldsymbol{J}}_D|_{\tilde{\boldsymbol{g}},\tilde{\boldsymbol{h}}}\right) \quad \text{s.t.} \quad \tilde{\boldsymbol{g}}^{\mathrm{H}}\tilde{\boldsymbol{g}} \leq P_T. \tag{97}$$

Note that in contrast to (18), the problem is now formulated based on the EFIM approximation $\bar{\boldsymbol{J}}_D$ that has been introduced in Section VI. In this section, we will present an algorithm which solves the maximization task (97).

To this end, we first focus on the simpler problem of optimizing the transmit signal $\tilde{\boldsymbol{g}}$ for a given receive filter $\tilde{\boldsymbol{h}}$

$$\max_{\tilde{\boldsymbol{g}}} \quad \mathrm{tr}\left(\boldsymbol{M}'\bar{\boldsymbol{J}}_D|_{\tilde{\boldsymbol{g}},\tilde{\boldsymbol{h}}}\right) \quad \text{s.t.} \quad \tilde{\boldsymbol{g}}^{\mathrm{H}}\tilde{\boldsymbol{g}} \leq P_T, \tag{98}$$

where the cost function is expressed in the form (65). It is well known that the solution to such a problem is the Eigenvector $\boldsymbol{\gamma}_1$ of the matrix $\boldsymbol{\Phi}$ corresponding to the largest Eigenvalue.

On the other hand, for a constant transmit signal $\tilde{\boldsymbol{g}}$, the optimization problem reads as

$$\max_{\tilde{\boldsymbol{h}}} \quad \mathrm{tr}\left(\boldsymbol{M}'\bar{\boldsymbol{J}}_D|_{\tilde{\boldsymbol{g}},\tilde{\boldsymbol{h}}}\right). \tag{99}$$

Having a closer look at the filter representation of the objective function (72), it is straightforward to prove that two different vectors $\tilde{\boldsymbol{h}}_{k_1}$ and $\tilde{\boldsymbol{h}}_{k_2}$, $k_1 \neq k_2$ consist of two disjoint sets of filter coefficients H_k. Therefore problem (99) is solved by independently maximizing each term of the sum (96), which results in choosing $\tilde{\boldsymbol{h}}_k = \boldsymbol{\delta}_{k,1}$ where $\boldsymbol{\delta}_{k,1}$ is the Eigenvector of $\boldsymbol{\Delta}_k$ corresponding to the largest Eigenvalue.

With the two separate optimization tasks (98) and (99) for the transmit and the receive filter, we suggest the following iterative algorithm to find the solution to the design problem in (97). The algorithm is initialized with filters $\tilde{\boldsymbol{g}}_{\mathrm{init}}$ and $\tilde{\boldsymbol{h}}_{\mathrm{init}}$ that can either be chosen randomly or set to initial prototype versions. In an alternating way, in the i-th iteration the analog transmit filter $\tilde{\boldsymbol{g}}$ is optimized by solving (98) for a fixed receive filter $\tilde{\boldsymbol{h}}^{i-1}$. The solution $\tilde{\boldsymbol{g}}^i$ is then used as a constant in order to improve the solution for $\tilde{\boldsymbol{h}}$ with (99). This approach ensures that the value of the objective function increases with each iteration. If the relative performance gain is less than a threshold value ϵ, the algorithm terminates and outputs the solutions $\tilde{\boldsymbol{g}}^\star$ and $\tilde{\boldsymbol{h}}^\star$. Note that such an alternating approach does not necessarily find the globally optimum solution. However, as simulations will show (see Sections X and XI), the procedure outputs a transceiver design which provides significant performance gains. For all tested scenarios, the suggested algorithm converges quickly and returns a favorable design after a few steps.

IX. Reference Systems

In order to provide a comparison to commonly used system designs, we introduce two references which will serve as a benchmark for the optimized transceiver. We use rectangular pulses as employed in Global Navigation Satellite Systems (GNSS) [49] such as the American Global Positioning System (GPS) or the European Galileo GNSS system, and linear frequency modulation (LFM) pulses that find application in radar systems which demand a long range and high resolution [50, p. 88]. For further details about LFM pulses, the reader is referred to [51].

Both of the above transmit signals $\breve{x}(t)$ can be described by the periodic repetition of the transmit pulse $g(t)$ in intervals of T_0. Having available the spectrum $G(\omega)$ of the reference pulse, the transmit filter Fourier coefficients are simply obtained by the evaluation of the discrete spectrum points $G(k\omega_0)$ and normalizing to $\tilde{\boldsymbol{g}}_{\mathrm{ref}}^{\mathrm{H}}\tilde{\boldsymbol{g}}_{\mathrm{ref}} = P_T$. The analog reference receive filter $\tilde{\boldsymbol{h}}_{\mathrm{ref}}$ is an ideal low-pass filter with bandwidth $B_{\mathrm{ref}} = f_s$ which complies with the sampling theorem. In order to visualize the possible performance gains, in the following we consider the relative performance measures

$$\chi_{\tau/\nu} = 10\log\left(\frac{\left[\boldsymbol{J}_D^{-1}|_{\tilde{\boldsymbol{g}}_{\mathrm{ref}},\tilde{\boldsymbol{h}}_{\mathrm{ref}}}\right]_{11/22}}{\left[\boldsymbol{J}_D^{-1}|_{\tilde{\boldsymbol{g}},\tilde{\boldsymbol{h}}}\right]_{11/22}}\right), \tag{100}$$

which characterize the information gain in the measurement influenced part of the BCRLB (10) and therefore measure the factor by which the transmit power of the optimized system could be reduced while maintaining the performance from the reference system. Note that (100) is computed using the exact EFIM (11). The reference systems are configured such that they use the same transmit power P_T and have the same period T_0 like the optimized system.

A. Rectangular Phase Code Modulation

The rectangular prototype pulse has duration $T = 2T_s$ and its Fourier transform can be denoted

$$g_{\mathrm{Rect}}^{(\infty)}(t) = \mathrm{rect}\left(\frac{t}{T}\right), \tag{101}$$

$$G_{\mathrm{Rect}}^{(\infty)}(\omega) = \frac{2\sin\left(\omega\frac{T}{2}\right)}{\omega}. \tag{102}$$

Under the assumption that the pulse is ideally band-limited at the transmitter to a two-sided bandwidth $B = f_s$, we obtain

$$G_{\mathrm{Rect}}(\omega) = \begin{cases} \frac{2\sin\left(\omega\frac{T}{2}\right)}{\omega}, & -\pi B \leq \omega < \pi B \\ 0, & \text{otherwise} \end{cases}, \tag{103}$$

$$g_{\mathrm{Rect}}(t) = \int g_{\mathrm{Rect}}^{(\infty)}(\psi)\frac{\sin\left(\pi B(t-\psi)\right)}{\pi(t-\psi)}\mathrm{d}\psi. \tag{104}$$

The rectangular phase code (RPC) is then generated by convolving the prototype rectangular pulse with a code sequence

$$g_{\mathrm{RPC}}(t) = g_{\mathrm{Rect}}(t) * \beta(t), \tag{105}$$

where

$$\beta(t) = \sum_{m=0}^{M-1} \beta_m \delta(t - mT) \tag{106}$$

for some binary sequence $\beta_m \in \{-1, 1\}$.

B. Linear Frequency Modulation (LFM)

The LFM reference signal consists of an envelope $a_{\mathrm{LFM}}(t)$ and a sinusoid with linearly increasing frequency $w_{\mathrm{LFM}}(t)$. For the case of a rectangular envelope, we have

$$a_{\mathrm{LFM}}(t) = \mathrm{rect}\left(\frac{t}{T}\right), \tag{107}$$

$$w_{\mathrm{LFM}}(t) = \mathrm{e}^{\mathrm{j}\frac{\mu t^2}{2}}, \tag{108}$$

with pulse duration T and frequency slope μ. In the literature, (108) is often referred to as chirp pulse. The frequency of the sinusoid is increasing linearly in time

$$\omega = \frac{\mathrm{d}\angle(w_{\mathrm{LFM}}(t))}{\mathrm{d}t} = \mu t. \tag{109}$$

The LFM transmit pulse and its spectrum are [50, p. 138]

$$g_{\mathrm{LFM}}(t) = a_{\mathrm{LFM}}(t) w_{\mathrm{LFM}}(t) \tag{110}$$

$$G_{\mathrm{LFM}}(\omega) = \frac{1}{2}\sqrt{\frac{\pi}{\mu}} \mathrm{e}^{-\mathrm{j}\frac{\omega^2}{2\mu}} \left[Z\left(\sqrt{\frac{1}{\pi\mu}}\omega + \sqrt{\frac{\mu T^2}{4\pi}}\right) + Z\left(-\sqrt{\frac{1}{\pi\mu}}\omega + \sqrt{\frac{\mu T^2}{4\pi}}\right) \right], \tag{111}$$

with the complex Fresnel integral $Z(u) = \int_0^u \mathrm{e}^{\mathrm{j}\pi\frac{a^2}{2}}\mathrm{d}a$. The two-sided bandwidth of this pulse is approximately $B_{\mathrm{LFM}} = \frac{\mu T}{2\pi}$. For the reference system, we use a pulse length of $T = T_0$. The bandwidth $B_{\mathrm{LFM}} = \frac{2f_s}{3}$ uses the full frequency band without violating the sampling theorem and yields $\mu = \frac{4\pi N}{3T_0^2}$.

X. Optimization Results

A. Performance - Pareto-optimal Transceiver Region

In general there exists a trade-off between the estimation accuracy of the time-delay and the Doppler shift. As such, for the presented transceiver optimization framework we examine the Pareto-optimal set $\mathcal{P}$ of joint transmit and receive filters, $\mathcal{P} = \{(g(t), h(t))\}$, for which the estimation of one channel parameter cannot be improved by changing the filters without reducing the accuracy of the other parameter. We define the associated set $\mathcal{G}$ of relative performance gains (100) that are obtained by filters on the boundary of the Pareto-optimal region $\mathcal{P}$ as

$$\mathcal{G} = \left\{ (\chi_\tau, \chi_\nu)\big|_{\mathcal{P}} \right\}. \tag{112}$$

It can be approximated by solving the transceiver optimization problem (97) over all positive definite weighting matrices $\boldsymbol{M}'$ and computing the corresponding EFIM values (11). In section VII-B it has been shown that for the examined system the non-diagonal elements of the EFIM $\bar{\boldsymbol{J}}_D$ vanish and it is therefore sufficient to consider diagonal weighting matrices

$$\boldsymbol{M}' = \mathrm{diag}(\alpha, 1-\alpha), \tag{113}$$

with $\alpha \in [0, 1]$.

1) Variable Bandwidth with Fixed Sampling Rate: Fig. 2 shows the Pareto boundary for different bandwidths $B = (2L+1)f_s$ and signal periods T_0, where $f_s = 25\mathrm{MHz}$ has been used. Here, the rectangular transmit waveform (105) is used as the reference in (100) and the variances of the random unknown channel parameters (22) are set to $\sigma_\tau = 1\mathrm{ns}, \sigma_\nu = 5\mathrm{kHz}$. Fig. 2 has been created by solving (18) for symmetric signals under all weightings α and computing the corresponding exact values $\chi_{\tau/\nu}$ (100). It can be observed that for the estimation of the time-delay τ, increasing the bandwidth L leads to a substantial performance gain, while for the estimation of the Doppler, extension of the time-spread T_0 improves the achievable accuracy. The fact that the Pareto region appears to be larger for the Doppler parameter when the bandwidth is lower can be explained by the inaccuracies that result from the approximation of the EFIM used in (97). We see that for essentially any choice of the weighting matrix, the optimized design provides significant gains in estimation performance compared with the prototypes. We also note that the nearly rectangular Pareto regions indicate that, with optimized filter designs, the trade-off between delay and Doppler estimation performance is relatively small.

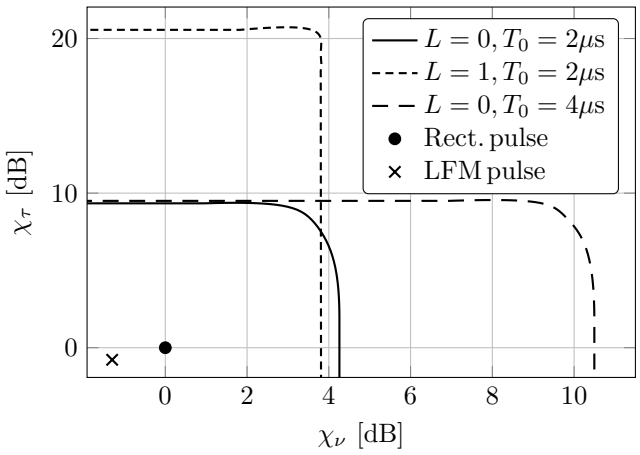

Fig. 2. Pareto regions for bandwidths $B = (2L+1)f_s$ and signal periods T_0 with $f_s = 25\mathrm{MHz}$

2) Fixed Bandwidth with Variable Sampling Rate: We have seen that optimized filters have the potential to increase the estimation performance of delay-Doppler estimation methods. We now investigate the estimation performance for a fixed transmit bandwidth $B = 25\mathrm{MHz}$, a signal period $T_0 = 2.4\mu\mathrm{s}$ and different sampling frequencies $f_s = \frac{B}{2L+1}$. Fig. 3 shows the Pareto regions of the optimized waveforms with respect to a rectangular signal, all with the same bandwidth of $B = 25\mathrm{MHz}$. Hence, the number of Fourier coefficients $K = BT_0$ is the same for all systems. Note that the sampling rate for the reference system is held constant, while the sampling rate and the number of samples N of the optimized system decreases with increasing L. This indicates that although lower sampling

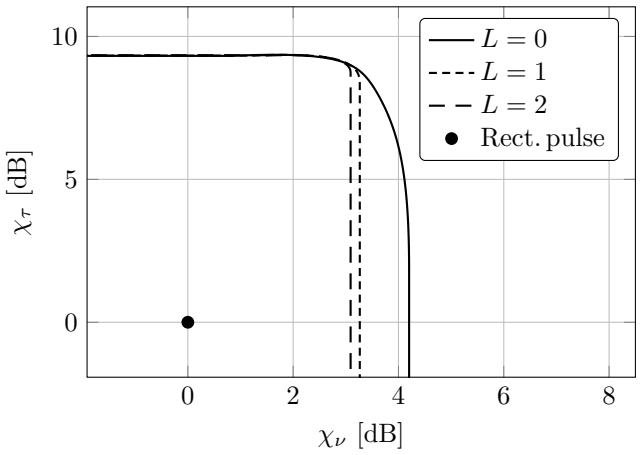

Fig. 3. Pareto regions for rates $f_s = \frac{B}{2L+1}$ with $B = 25\mathrm{MHz}$

rates are used, the optimized waveform design can still provide high estimation accuracy. In contrast to the expected behavior that the CRLB scales linearly with the number of samples N, the time delay estimation barely suffers from reducing the sampling rate as the power of the optimized transmit filter is concentrated around high frequencies, as we will see later, e.g., Fig. 5a. Further, a receive filter with bandpass structure filters out low-frequency noise for the undersampled systems, as observed in Fig. 5d. However, the Doppler estimation suffers slightly from a reduced number of sampling points.

B. Design - Optimized Transmit and Receive Filters

In order to illustrate transceiver designs optimized for the estimation of τ and ν, we visualize time and frequency domain representations of the analog receive and transmit filters obtained with the presented optimization algorithm. For the same configuration as in Fig. 2 and a signal period of $T_0 = 2\mu$s we first investigate the case where the sampling theorem is satisfied, i.e., $L = 0$. Note that under these conditions the optimum receive filter is an ideal rectangular band-pass filter with two-sided bandwidth f_s.

Fig. 4a shows the spectrum of the optimized transmit signal in the frequency-domain when full weight is given to the optimization of the delay estimation ($\alpha = 1$). In contrast Fig. 4b depicts the result of the transmit filter optimization in the time-domain when the inference of the Doppler is emphasized ($\alpha = 0$). It can be observed that when focusing on estimation of the delay ($\alpha = 1$), the transmit signal power is concentrated at high frequencies (see Fig. 4a). When enforcing estimation of the Doppler, the signal power is concentrated around the edges of the observation interval (see Fig. 4b). This is because for delay estimation, signal components with high frequencies are more beneficial for the EFIM, since the phase shift, which is introduced by the propagation delay, increases linearly in frequency. On the other hand, for Doppler estimation a signal with wide time-spread is beneficial as the phase shift that is introduced by the Doppler effect increases linearly in time. Using a weighting

$$\alpha^\star = \arg \max_{0<\alpha<1} \chi_\tau + \chi_\nu, \tag{114}$$

which simultaneously emphasizes both the estimation of the delay and Doppler shift, we obtain the transmit filter depicted in Figs. 4c and 4d. Note that α^* leads to the point on $\mathcal{G}$ at which the sum of both accuracy gains (100) is maximum, i.e., the most upper right point in the Pareto region $\mathcal{G}$. It can be observed that in this case, the signal power is concentrated at the boundaries of the time and frequency domain. Due to the properties of the Fourier transform, the signal cannot simultaneously be concentrated in both time and frequency, which leads to the observed trade-off between delay and Doppler estimation. Furthermore, it is noticeable that the optimized transmit signal exhibits strong oscillations in the time and frequency domain (Figs. 4c and 4d). Allowing for a higher bandwidth $L = 1$, i.e., $B = 3f_s$ and therefore for receive signals which violate the sampling theorem, Figs. 5a and 5b show the optimized waveform for the max-sum weighting $\alpha^\star$ (114). The dashed lines visualize the interval $[-\frac{\omega_s}{2}, \frac{\omega_s}{2})$. It can be observed that the optimized transmit filter has a total bandwidth of $B > f_s$ and therefore violates the sampling theorem. However, as this signal shows a bandpass character, the real bandwidth of the signal, i.e., the cumulative portion of the frequencies where the signal exhibits non-zero spectral power density is merely ω_s. Although the total bandwidth of the signal exceeds ω_s, due to its bandpass character the transmit signal does not experience significant aliasing during the sampling process at the receiver. Comparing the sampled

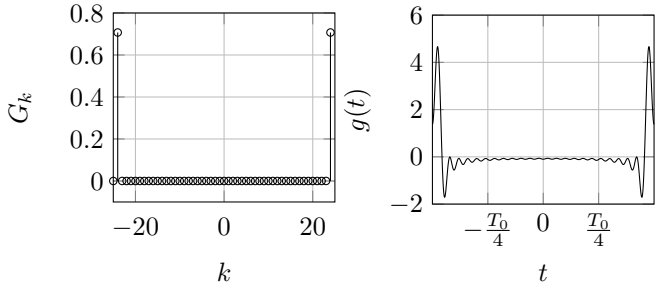

(a) Frequency domain ($\alpha = 1$) (b) Time domain ($\alpha = 0$)

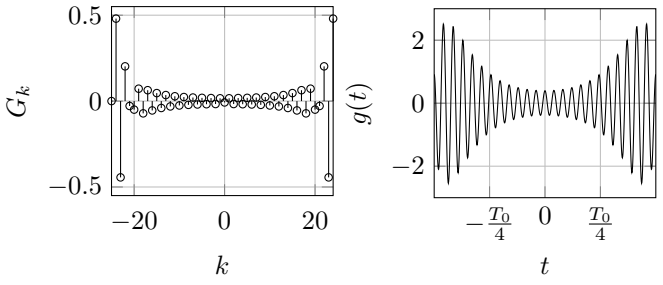

(c) Frequency domain ($\alpha = \alpha^\star$) (d) Time domain ($\alpha = \alpha^\star$)

Fig. 4. Optimized transmit filters ($L = 0$)

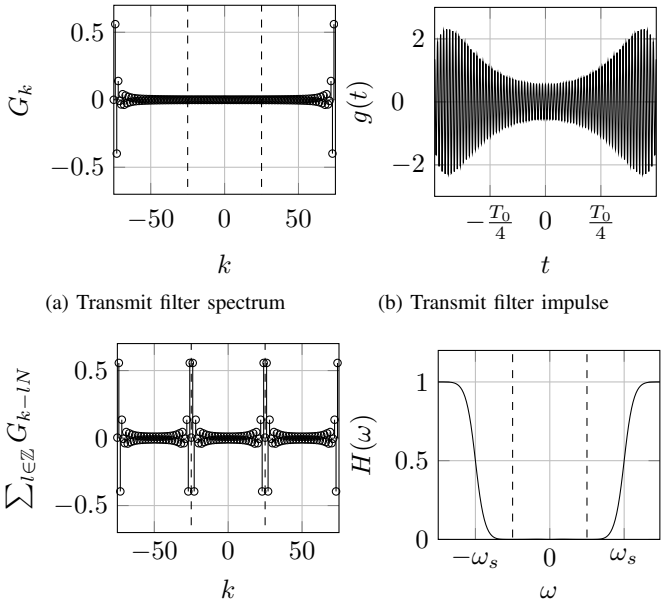

(a) Transmit filter spectrum (b) Transmit filter impulse

(c) Periodic transmit filter spectrum (d) Receive filter spectrum

Fig. 5. Optimized transmit and receive filters ($L = 1, \alpha = \alpha^\star$)

signal spectrum in Fig. 5c with the transmit spectrum in Fig. 5a, it can be seen that signal replicas are not distorted. The advantage of the bandpass character of the transmitter is a high sensitivity at the receiver with respect to the propagation delay. Fig. 5d displays the optimized receive filter spectrum, which is a bandpass. An interesting observation is that none of the optimized signals uses the full available bandwidth B. Note that due to the relatively small prior variances, in general the full bandwidth and time interval could be used. For higher parameter uncertainties, safety margins at the interval boundaries would occur in order to prevent a potential power loss from high frequency or time shifts.

C. Complexity - Ambiguity Function

The ambiguity function, defined as the output of a matched filter without Doppler shift compensation

$$\psi(\boldsymbol{\theta}) = \left| \int_{-\infty}^{\infty} \breve{x}(t)\breve{x}^*(t+\tau)\mathrm{e}^{\mathrm{j}2\pi\nu t}\mathrm{d}t \right|^2, \tag{115}$$

is a well-known indicator for analyzing the suitability of transmit waveforms for delay-Doppler estimation [50, ch. 4]. It can be shown that (115) is directly related to the functional distance of the transmit waveform and its time and frequency-shifted versions. It therefore provides insight about the similarity of the signal and its sensitivity with respect to shifts in time and frequency. By discussing the curvature of (115) at $\psi(0,0)$ and its side-lobe levels, it is possible to establish a measure of the adequateness of a waveform with respect to delay and Doppler estimation [52].

1) MAP Estimation: In a realistic scenario the attenuation γ in the receive signal model (19) is deterministic and unknown, so the joint maximum-a-posteriori/maximum-likelihood (JMAP-ML) approach [53]

$$\begin{bmatrix} \hat{\gamma}_{\mathrm{ML}}(\boldsymbol{y}) \\ \hat{\boldsymbol{\theta}}_{\mathrm{MAP}}(\boldsymbol{y}) \end{bmatrix} = \arg\max_{\boldsymbol{\theta},\gamma} \big(\ln p(\boldsymbol{y}|\boldsymbol{\theta},\gamma) + \ln p(\boldsymbol{\theta}) \big) \tag{116}$$

has to be used in order to estimate the channel parameters. For the case of Gaussian noise, the likelihood function becomes

$$p(\boldsymbol{y}|\boldsymbol{\theta},\gamma) \propto \exp\Big(-\frac{1}{2} \big(\boldsymbol{y} - \boldsymbol{v}(\boldsymbol{\theta},\gamma)\big)^{\mathrm{H}} \boldsymbol{R}_{\boldsymbol{\eta}}^{-1} \big(\boldsymbol{y} - \boldsymbol{v}(\boldsymbol{\theta},\gamma)\big) \Big). \tag{117}$$

Writing

$$\boldsymbol{v}(\boldsymbol{\theta},\gamma) = \gamma \boldsymbol{s}(\boldsymbol{\theta}), \tag{118}$$

we find that the solution of (116) needs to satisfy

$$\frac{\partial}{\partial \gamma^*} \ln p(\boldsymbol{y}|\boldsymbol{\theta},\gamma) = \boldsymbol{s}^{\mathrm{H}}(\boldsymbol{\theta}) \boldsymbol{R}_{\boldsymbol{\eta}}^{-1} \left(\boldsymbol{y} - \gamma \boldsymbol{s}(\boldsymbol{\theta})\right) = 0. \tag{119}$$

Hence, we obtain the estimator for the channel coefficient

$$\hat{\gamma}(\boldsymbol{\theta}) = \frac{\boldsymbol{s}^{\mathrm{H}}(\boldsymbol{\theta}) \boldsymbol{R}_{\boldsymbol{\eta}}^{-1} \boldsymbol{y}}{\boldsymbol{s}^{\mathrm{H}}(\boldsymbol{\theta}) \boldsymbol{R}_{\boldsymbol{\eta}}^{-1} \boldsymbol{s}(\boldsymbol{\theta})}, \tag{120}$$

as a function of the parameters $\boldsymbol{\theta}$. Substituting (120) into (116), we obtain the estimator

$$\begin{aligned} &\hat{\boldsymbol{\theta}}_{\mathrm{MAP}}(\boldsymbol{y}) = \\ &= \arg\max_{\boldsymbol{\theta}} \big(\ln p(\boldsymbol{y}|\boldsymbol{\theta}, \hat{\gamma}(\boldsymbol{\theta})) + \ln p(\boldsymbol{\theta}) \big) \\ &= \arg\max_{\boldsymbol{\theta}} \Big(- \big(\boldsymbol{y} - \hat{\gamma}(\boldsymbol{\theta}) \boldsymbol{s}(\boldsymbol{\theta})\big)^{\mathrm{H}} \boldsymbol{R}_{\boldsymbol{\eta}}^{-1} \big(\boldsymbol{y} - \hat{\gamma}(\boldsymbol{\theta}) \boldsymbol{s}(\boldsymbol{\theta})\big) \\ &\qquad - \frac{(\tau - \mu_\tau)^2}{\sigma_\tau^2} - \frac{(\nu - \mu_\nu)^2}{\sigma_\nu^2} \Big) \\ &= \arg\max_{\boldsymbol{\theta}} f_{\mathrm{MAP}}(\boldsymbol{\theta}), \end{aligned} \tag{121}$$

as the maximizer of the MAP function

$$f_{\mathrm{MAP}}(\boldsymbol{\theta}) = \frac{|\boldsymbol{s}^{\mathrm{H}}(\boldsymbol{\theta}) \boldsymbol{R}_{\boldsymbol{\eta}}^{-1} \boldsymbol{y}|^2}{\boldsymbol{s}^{\mathrm{H}}(\boldsymbol{\theta}) \boldsymbol{R}_{\boldsymbol{\eta}}^{-1} \boldsymbol{s}(\boldsymbol{\theta})} - \frac{(\tau - \mu_\tau)^2}{\sigma_\tau^2} - \frac{(\nu - \mu_\nu)^2}{\sigma_\nu^2}. \tag{122}$$

2) MAP Ambiguity Function: On the basis of (122), we define a function

$$\psi_{\mathrm{MAP}}(\boldsymbol{\theta}) = f_{\mathrm{MAP}}(\boldsymbol{\theta})|_{\boldsymbol{y}=\boldsymbol{s}(\boldsymbol{0})}, \tag{123}$$

closely related to the ambiguity function (115), which we refer to as the MAP ambiguity function (MAP-AF). This measure is derived by an estimation theoretic argument directly from the likelihood function and has the advantage of incorporating the prior knowledge about the unknown parameters $\boldsymbol{\theta}$ into the ambiguity function. Further, in contrast to the standard ambiguity function (115), the uncertainty about the attenuation γ as well as the effect of colored noise with covariance $\boldsymbol{R}_{\boldsymbol{\eta}}$ is considered by the suggested ambiguity characterization (123).

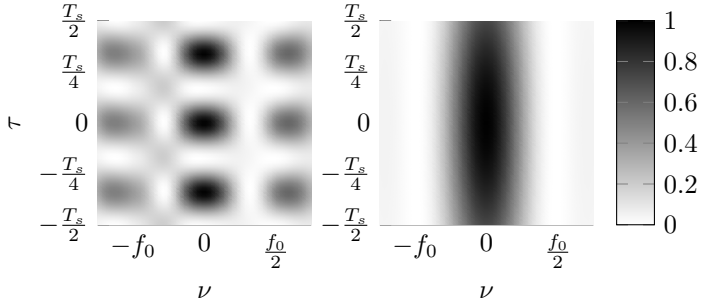

(a) Optimized ($L = 1$, $\alpha = \alpha^*$) (b) Rectangular

Fig. 6. MAP-AF for different transmit/receive filters

Figs. 6a and 6b show the normalized MAP-AF for the optimized transmit and receive filter and the reference LFM pulse (110) in a signal-dominant environment, i.e., $N_0 \to 0$ in order to highlight the effect of the transmit and receive filters. It can be seen that the optimized system exhibits a MAP-AF maximum that is significantly narrower than that of the LFM signal which allows for a higher time-delay and Doppler estimation accuracy. Note that the optimized system shows local maxima, which can cause ambiguities for the solution of the estimator (121). However, for a priori knowledge with small uncertainties, i.e., $\sigma_\nu \ll f_0$, $\sigma_\tau \ll T_s$, these local extrema do not influence the estimation as the probability that

a MAP-AF function side-lobe exceeds the main lobe for a particular noise realization vanishes.

XI. Simulation Results

With the estimator (121) it is possible to use Monte-Carlo simulations to verify the achievable performance gain with an optimized transceiver design. To this end, we use $f_s = 25\text{MHz}$ and $T_0 = 2\mu\text{s}$. The uncertainty of the time and Doppler shift are $\sigma_\tau = 1\text{ns}$ and $\sigma_\nu = 5\text{kHz}$ and $L = 1$. The optimized transmit and receive filters are obtained by using the max-sum weighting $\alpha^\star$ for the matrix $\boldsymbol{M'}$. Figs. 7 and 8 show the empirical normalized mean squared error (NMSE)

$$\text{NMSE}_{\hat{\tau}/\hat{\nu}} = \frac{\text{MSE}_{\hat{\tau}/\hat{\nu}}}{\sigma^2_{\tau/\nu}} \tag{124}$$

of the estimator (121) for the optimized and rectangular reference systems compared with the analytical BCRLB (10) on a double logarithmic scale, where $\text{MSE}_{\hat{\tau}/\hat{\nu}}$ represents the diagonal elements of (9), empirically evaluated based on the estimation in (116). Note that we use the per-Hz

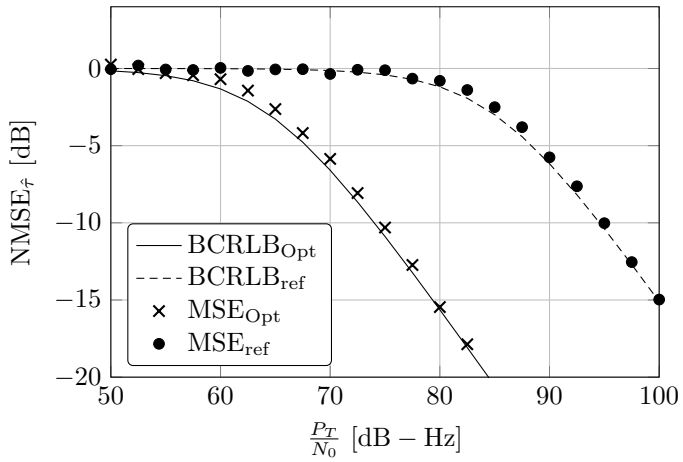

Fig. 7. MSE and BCRLB - Time-delay τ

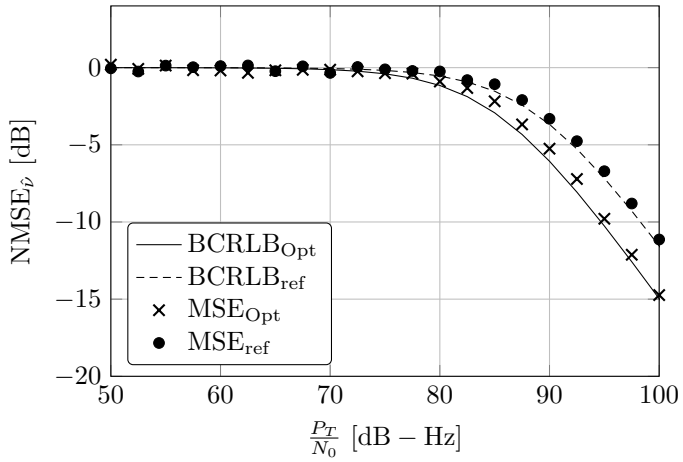

Fig. 8. MSE and BCRLB - Doppler shift ν

signal-to-noise ratio (pSNR) $\frac{P_T}{N_0}$ to establish a fair comparison between different transceive filters. For low pSNR, the BCRLB saturates since the receive data is so noisy that it does not contribute to the performance of the estimator (121). The estimator then exclusively operates on the basis of the prior information and simply produces the mean $\hat{\boldsymbol{\theta}} = \boldsymbol{\mu}_{\boldsymbol{\theta}}$. In the high pSNR regime, it can be observed that the RMSE of the estimator (121) converges to the BCRLB. In this region, the presented transmit and receive filter optimization is beneficial, as the estimator favors the received data in the estimation process. Furthermore, it is observed that for moderate to high pSNR values the performance gain is roughly 20dB for the estimation of the time-delay and 4dB for the Doppler estimation, which corresponds to the findings from the Pareto region in Fig. 2. The pSNR value at which the receive data starts to contribute to the reduction of the estimation uncertainty is approximately $\text{pSNR}_\tau = 65\text{dB} - \text{Hz}$ for the time-delay and $\text{pSNR}_\nu = 85\text{dB} - \text{Hz}$ for the Doppler shift. The difference between these two pSNR levels can be explained by the different sensitivity of the transceiver with respect to the two channel parameters. Note that when observing multiple periods T_0 of the transmit signal, the estimation accuracy of the time-delay increases linearly with T_0. In contrast, the Doppler shift performance grows quadratically with T_0, since the sensitivity of the receive signal on the Doppler phase shift scales linearly with the observation interval. As a consequence, the gap between pSNR_τ and pSNR_ν can be eliminated by using a larger sampling period T_0.

XII. Conclusion

In this work, we have presented a framework for the joint optimization of the analog transmit and receive filters for estimating the time and Doppler shift of a propagation channel. The initial weighted MSE minimization problem has been reformulated as a maximization problem based on the expected Fisher information matrix. Exploiting various approximations, we have shown that it is possible to find transceiver filters that perform significantly better than conventional designs using a simple optimization algorithm. We showed that the resulting waveforms exhibit bandwidths that violate the sampling theorem ($B > f_s$), while the obtained filters have a bandpass structure which captures the entire signal power of the transmit waveform. The Pareto-optimal region exhibits a minimal trade-off between delay and Doppler estimation and is substantially increased by jointly optimizing the transmit and receive filters. Further, we have modified the standard ambiguity function in order to take into account prior information on the delay and Doppler parameters, and illustrated the gain of our optimized system relative to conventional approaches using the resulting MAP ambiguity function. In order to evaluate the performance of the adapted transceiver, Monte-Carlo simulations were performed. The simulation results show significant accuracy gains, such that we conclude that transceiver optimization is necessary in order to design channel estimation systems operating under sub-Nyquist conditions.

References

[1] R. H. Walden, "Analog-to-digital converter survey and analysis," *IEEE J. Sel. Areas Commun.*, vol. 17, no. 4, pp. 539–550, Apr. 1999.

[2] M. Verhelst and A. Bahai, "Where analog meets digital: Analog-to-information conversion and beyond," *IEEE Solid-State Circuits Mag.*, vol. 7, no. 3, pp. 67–80, Sep. 2015.

[3] H. L. V. Trees and K. L. Bell, *Bayesian Bounds for Parameter Estimation and Nonlinear Filtering/Tracking*. Piscataway, NJ: Wiley-IEEE Press, 2007.

[4] S. M. Kay, *Fundamentals of Statistical Signal Processing: Estimation Theory*. Upper Saddle River, NJ: Prentice Hall, 1993.

[5] M. Stein, M. Castaneda, A. Mezghani, and J. Nossek, "Information-preserving transformations for signal parameter estimation," *IEEE Signal Process. Lett.*, vol. 21, no. 7, pp. 866–870, Jul. 2014.

[6] M. Stein, A. Lenz, A. Mezghani, and J. Nossek, "Optimum analog receive filters for detection and inference under a sampling rate constraint," in *IEEE Int. Conf. Acoustics, Speech and Signal Processing (ICASSP)*, Florence, Italy, May 2014, pp. 1827–1831.

[7] A. Lenz, M. Stein, and J. A. Nossek, "Signal parameter estimation performance under a sampling rate constraint," in *49th Asilomar Conf. Signals, Systems and Computers*, Pacific Grove, CA, Nov. 2015, pp. 503–507.

[8] A. Lenz, M. Stein, and A. L. Swindlehurst, "Analog transmit signal optimization for undersampled delay-Doppler estimation," *pre-print*, 2017. [Online]. Available: https://arxiv.org/abs/1703.06858

[9] M. Khayambashi and A. L. Swindlehurst, "Filter design for a compressive sensing delay and Doppler estimation framework," in *48th Asilomar Conf. Signals, Systems and Computers*, Pacific Grove, CA, Nov. 2014, pp. 627–631.

[10] Y. Yang and R. S. Blum, "Minimax robust MIMO radar waveform design," *IEEE J. Sel. Topics Signal Process.*, vol. 1, no. 1, pp. 147–155, Jun. 2007.

[11] S. Haykin, Y. Xue, and T. N. Davidson, "Optimal waveform design for cognitive radar," in *42nd Asilomar Conf. Signals, Systems and Computers*, Pacific Grove, CA, Oct. 2008, pp. 3–7.

[12] R. A. Romero, J. Bae, and N. A. Goodman, "Theory and application of SNR and mutual information matched illumination waveforms," *IEEE Trans. Aerosp. Electron. Syst.*, vol. 47, no. 2, pp. 912–927, Apr. 2011.

[13] P. Stoica, H. He, and J. Li, "Optimization of the receive filter and transmit sequence for active sensing," *IEEE Trans. Signal Process.*, vol. 60, no. 4, pp. 1730–1740, Apr. 2012.

[14] M. R. Bell, "Information theory and radar waveform design," *IEEE Trans. Inf. Theory*, vol. 39, no. 5, pp. 1578–1597, Apr. 1993.

[15] J. R. Guerci and S. U. Pillai, "Theory and application of optimum transmit-receive radar," in *IEEE Int. Radar Conf.*, Alexandria, VA, May 2000, pp. 705–710.

[16] R. Calderbank, S. D. Howard, and B. Moran, "Waveform diversity in radar signal processing," *IEEE Signal Process. Mag.*, vol. 26, no. 1, pp. 32–41, Jan. 2009.

[17] C. R. Berger, B. Demissie, J. Heckenbach, P. Willett, and S. Zhou, "Signal processing for passive radar using OFDM waveforms," *IEEE J. Sel. Topics Signal Process.*, vol. 4, no. 1, pp. 226–238, Feb. 2010.

[18] F. Antreich, "Array processing and signal design for timing synchronization," Ph.D. dissertation, Technical University of Munich, 2011.

[19] E. Fishler, A. Haimovich, R. Blum, D. Chizhik, L. Cimini, and R. Valenzuela, "MIMO radar: An idea whose time has come," in *IEEE Radar Conf.*, Philadelphia, PA, Apr. 2004, pp. 71–78.

[20] P. Stoica, J. Li, and Y. Xie, "On probing signal design for MIMO radar," *IEEE Trans. Signal Process.*, vol. 55, no. 8, pp. 4151–4161, Aug. 2007.

[21] S. Haykin, "Cognitive radar: A way of the future," *IEEE Signal Process. Mag.*, vol. 23, no. 1, pp. 30–40, Jan. 2006.

[22] W. Huleihel, J. Tabrikian, and R. Shavit, "Optimal adaptive waveform design for cognitive MIMO radar," *IEEE Trans. Signal Process.*, vol. 61, no. 20, pp. 5075–5089, Oct. 2013.

[23] D. W. Bliss and K. W. Forsythe, "Multiple-input multiple-output (MIMO) radar and imaging: Degrees of freedom and resolution," in *37th Asilomar Conf. on Signals, Systems and Computers*, Pacific Grove, CA, Nov. 2003, pp. 54–59.

[24] J. Li and P. Stoica, "MIMO radar with colocated antennas," *IEEE Signal Process. Mag.*, vol. 24, no. 5, pp. 106–114, Sep. 2007.

[25] A. Leshem, O. Naparstek, and A. Nehorai, "Information theoretic adaptive radar waveform design for multiple extended targets," *IEEE J. Sel. Topics Signal Process.*, vol. 1, no. 1, pp. 42–55, Jun. 2007.

[26] J. Li, L. Xu, P. Stoica, K. W. Forsythe, and D. W. Bliss, "Range compression and waveform optimization for MIMO radar: A Cramér-Rao bound based study," *IEEE Trans. Signal Process.*, vol. 56, no. 1, pp. 218–232, Jan. 2008.

[27] M. Hurtado, T. Zhao, and A. Nehorai, "Adaptive polarized waveform design for target tracking based on sequential Bayesian inference," *IEEE Trans. Signal Process.*, vol. 56, no. 3, pp. 1120–1133, Mar. 2008.

[28] C. Wilcox, "The synthesis problem for radar ambiguity functions," Math. Res. Center, U.S. Army, Univ. Wisconsin, Madison, WI, MRC Tech. Summary Rep. 157, Apr. 1960.

[29] C. Knapp and G. Carter, "The generalized correlation method for estimation of time delay," *IEEE Trans. Acoust., Speech, Signal Process.*, vol. 24, no. 4, pp. 320–327, Aug. 1976.

[30] S. Stein, "Algorithms for ambiguity function processing," *IEEE Trans. Acoust., Speech, Signal Process.*, vol. 29, no. 3, pp. 588–599, Aug. 1981.

[31] G. S. Antonio, D. R. Fuhrmann, and F. C. Robey, "MIMO radar ambiguity functions," *IEEE J. Sel. Topics Signal Process.*, vol. 1, no. 1, pp. 167–177, Jun. 2007.

[32] C. Y. Chen and P. P. Vaidyanathan, "MIMO radar ambiguity properties and optimization using frequency-hopping waveforms," *IEEE Trans. Signal Process.*, vol. 56, no. 12, pp. 5926–5936, Dec. 2008.

[33] A. L. Swindlehurst and P. Stoica, "Maximum likelihood methods in radar array signal processing," *Proc. IEEE*, vol. 86, no. 2, pp. 421–441, Feb. 1998.

[34] A. Jakobsson, A. L. Swindlehurst, and P. Stoica, "Subspace-based estimation of time delays and Doppler shifts," *IEEE Trans. Signal Process.*, vol. 46, no. 9, pp. 2472–2483, Sep. 1998.

[35] D. Donoho, "Compressed sensing," *IEEE Trans. Inf. Theory*, vol. 52, no. 4, pp. 1289–1306, Apr. 2006.

[36] M. Vetterli, P. Marziliano, and T. Blu, "Sampling signals with finite rate of innovation," *IEEE Trans. Signal Process.*, vol. 50, no. 6, pp. 1417–1428, Jun. 2002.

[37] E. Candes and M. Wakin, "An introduction to compressive sampling," *IEEE Signal Process. Mag.*, vol. 25, no. 2, pp. 21–30, Mar. 2008.

[38] X. Wei and P. L. Dragotti, "Universal sampling of signals with finite rate of innovation," in *IEEE Int. Conf. Acoustics, Speech and Signal Processing (ICASSP)*, Florence, Italy, May 2014, pp. 1803–1807.

[39] I. Maravic and M. Vetterli, "Sampling and reconstruction of signals with finite rate of innovation in the presence of noise," *IEEE Trans. Signal Process.*, vol. 53, no. 8, pp. 2788–2805, Aug. 2005.

[40] V. Y. F. Tan and V. K. Goyal, "Estimating signals with finite rate of innovation from noisy samples: A stochastic algorithm," *IEEE Trans. Signal Process.*, vol. 56, no. 10, pp. 5135–5146, Oct. 2008.

[41] Z. Ben-Haim, T. Michaeli, and Y. C. Eldar, "Performance bounds and design criteria for estimating finite rate of innovation signals," *IEEE Trans. Inf. Theory*, vol. 58, no. 8, pp. 4993–5015, Aug. 2012.

[42] M. Davenport, P. Boufounos, M. Wakin, and R. Baraniuk, "Signal processing with compressive measurements," *IEEE J. Sel. Topics Signal Process.*, vol. 4, no. 2, pp. 445–460, Apr. 2010.

[43] M. Mishali, Y. C. Eldar, and A. J. Elron, "Xampling: Signal acquisition and processing in union of subspaces," *IEEE Trans. Signal Process.*, vol. 59, no. 10, pp. 4719–4734, Oct. 2011.

[44] T. Michaeli and Y. C. Eldar, "Xampling at the rate of innovation," *IEEE Trans. Signal Process.*, vol. 60, no. 3, pp. 1121–1133, Mar. 2012.

[45] M. Mishali, Y. C. Eldar, O. Dounaevsky, and E. Shoshan, "Xampling: Analog to digital at sub-Nyquist rates," *IET Circuits, Devices Systems*, vol. 5, no. 1, pp. 8–20, Jan. 2011.

[46] E. Baransky, G. Itzhak, N. Wagner, I. Shmuel, E. Shoshan, and Y. Eldar, "Sub-Nyquist radar prototype: Hardware and algorithm," *IEEE Trans. Aerosp. Electron. Syst.*, vol. 50, no. 2, pp. 809–822, Apr. 2014.

[47] A. Zeira and A. Nehorai, "Frequency domain Cramér-Rao bound for Gaussian processes," *IEEE Trans. Acoust., Speech, Signal Process.*, vol. 38, no. 6, pp. 1063–1066, Jun. 1990.

[48] U. Grenander and G. Szego, *Toeplitz Forms and their Applications*. University of California Press, 1958.

[49] P. Misra and P. Enge, *Global Positioning System: Signals, Measurements, and Performance*. Ganga-Jamuna Press, 2001.

[50] C. Cook, *Radar Signals: An Introduction to Theory and Application*. Artech Print on Demand, 1993.

[51] J. R. Klauder, A. C. Price, S. Darlington, and W. J. Albersheim, "The theory and design of chirp radars," *Bell Syst. Tech. J.*, vol. 39, no. 4, pp. 745–808, Jul. 1960. [Online]. Available: http://dx.doi.org/10.1002/j.1538-7305.1960.tb03942.x

[52] H. Gu, "Ambiguity function and Cramér-Rao bound in the multisignal case," *IEE Proc. - radar, sonar and navigation*, vol. 143, no. 4, pp. 227–231, Aug. 1996.

[53] A. Yeredor, "The joint MAP-ML criterion and its relation to ML and to extended least-squares," *IEEE Trans. Signal Process.*, vol. 48, no. 12, pp. 3484–3492, Dec. 2000.